



Transducer Elements Made from Piezoelectric Stacks

Pisan Sukwisut

**A Thesis Submitted in Partial Fulfillment of the Requirements for the Degree of
Master of Science in Physics
Prince of Songkla University
2009**

Copyright of Prince of Songkla University

Thesis Title Transducer Elements Made from Piezoelectric Stacks
Author Mr. Pisan Sukwisut
Major Program Physics

Major Advisor

.....
(Assoc. Prof. Dr. Supasarote Muensit)

Examining Committee:

.....Chairperson
(Asst. Prof. Dr. Pruittikorn Smithmaitrie)

.....
(Assoc. Prof. Dr. Supasarote Muensit)

.....
(Asst. Prof. Dr. Chitnarong Sirisathitkul)

The Graduate School, Prince of Songkla University, has approved this thesis as partial fulfillment of the requirements for the Master of Science Degree in Physics

.....
(Assoc. Prof. Dr. Kerekchai Thongnoo)
Dean of Graduate School

ชื่อวิทยานิพนธ์	วัสดุทรานสดิวเซอร์ผลิตจากสารไพเอโซอิเล็กทริกชั้นหลายชั้น
ผู้เขียน	นายพิศาล สุขวิสูตร
สาขาวิชา	ฟิสิกส์
ปีการศึกษา	2551

บทคัดย่อ

งานวิจัยนี้เตรียมวัสดุคอมโพสิต BaTiO₃-PVDF ที่มี PVDF เป็นเมทริกซ์และมีเซรามิก BaTiO₃ เติมเป็นสัดส่วนโดยปริมาตร 0.15 มีการขึ้นรูปสารด้วยวิธีหล่อแบบเทปก่อนผ่านกระบวนการโพลิงด้วยเงื่อนไขแตกต่างกันดังนี้ 1) โพลเฉพาะเฟส PVDF และ 2) โพลทั้ง 2 เฟส (ในทิศทางตรงข้ามกัน) ที่ความถี่ 1 kHz ค่าคงที่ได้ของอิเล็กทริกของสารตัวอย่างที่ผ่านการโพลิงทั้งสองแบบข้างต้นมีค่า 8.622 และ 8.753 ตามลำดับ (เท่ากับ 6.8 ในตัวอย่างที่ไม่โพล) ค่าสูญเสียไดอิเล็กทริกที่ต่ำที่สุดเท่ากับ 0.013 ได้จากสารตัวอย่างที่โพลทั้งสองเฟส จากนั้นทำสารไพเอโซอิเล็กทริกโดยการซ้อนคอมโพสิตกันตั้งแต่ 1 2 3 และ 4 ชั้น ศึกษาความถี่เรโซแนนซ์ และแอนติเรโซแนนซ์ด้วยวิธีการเรโซแนนซ์ สำหรับสารที่มี PVDF โพลเพียงเฟสเดียว มีความสัมพันธ์ระหว่างความถี่ (f) กับจำนวนชั้น (n) ตามสมการ $f = 107.59n + 269.54$ ซึ่งผลการวิเคราะห์ทางไฟไนต์อีลิเมนต์สอดคล้องกันกับผลการทดลองนี้ สำหรับสารมีการโพลทั้งสองเฟส คาดว่ามีความสัมพันธ์เชิงเส้นเช่นเดียวกันแต่ขนาดของค่าความชันและค่าตัดแกนแตกต่างกัน เมื่อนำความถี่ต่างๆที่วัดได้ไปคำนวณค่าสัมประสิทธิ์คัปปลิงทางไฟฟ้ากล พบว่าสารไพเอโซอิเล็กทริกของกรณีที่โพลเฉพาะ PVDF มีค่านี้ลดลงเมื่อจำนวนชั้นเพิ่มขึ้น ในขณะที่โพลทั้งสองเฟสตรงข้ามกัน ค่าสัมประสิทธิ์นี้เพิ่มขึ้นบ้างเล็กน้อยตามจำนวนชั้น แสดงว่าสารไพเอโซอิเล็กทริกแบบนี้มีศักยภาพในการทำเป็นส่วนพื้นฐานของทรานสดิวเซอร์

Thesis Title Transducer Elements Made from Piezoelectric Stacks
Author Mr.Pisan Sukwisut
Major Program Physics
Academic Year 2008

ABSTRACT

In this research, the BaTiO₃-PVDF composites in which a PVDF polymer was a matrix filled with 0.15 volume fraction of the BaTiO₃ ceramic were prepared. The composites were formed by a tape casting method and undergone different conditions during the corona poling process. The samples were poled in order to activate 1) only the PVDF, and 2) both the ceramic and polymer phases (pole oppositely). The dielectric constants at 1 kHz of the poled samples mentioned above were 8.622 and 8.753, respectively (6.8 for those unpoled). The dielectric loss (at 1 kHz) as low as 0.013 was obtained in the sample with both phases active. Subsequently, the piezoelectric stacks of 1, 2, 3 and 4 layers of the composites were made and the resonance method was used to observe the resonant and antiresonant frequencies of the stacks. For the piezoelectric stack with PVDF poled, a relationship between the observed frequencies (f) and number of the layers (n) in the stack was given as $f = 107.59n + 269.54$. The finite element analysis agreed well with experimental data. The stack with both phases poled was anticipated to have a similarly linear relationship, but, with a different sets of a slope and an intercept. The observed frequencies were used in the calculations of the electromechanical coupling coefficient of the piezoelectric stacks. The electromechanical coupling coefficient was decreased with number of the layers in the stack of only the PVDF poled. For the case of both phases poled oppositely, the coefficient was slightly increased with number of the layers. This suggested that the stack is attractive for use as transducer elements.

ACKNOWLEDGEMENT

I wish to express my sincere and deepest gratitude to my academic advisor Assoc. Prof. Dr. Supasarote Muensit for her constant help, personal attention, inspiring guidance, suggestions and encouragement given to me throughout the period of study, without which it would not have been possible for me to complete this work.

I would like to thank the examining committee for their suggestions: Asst. Prof. Dr. Pruittikorn Smithmaitrie and Asst. Prof. Dr. Chitnarong Sirisathitkul, for taking time out of their busy schedules to evaluate my work.

I show my gratitude for the helping hands from my friends in our research group, Mrs. Nawal Binhayeeniyi, Mr. Abedeen Dasaesamoh. I am indebted to my family, particularly to my mother for her kindness and endless care which always make me happy in mind without fear during an education.

Pisan Sukwisut

TABLES OF CONTENTS

ABSTRACT (Thai)	iii
ABSTRACT (English)	iv
ACKNOWLEDGEMENTS	v
TABLES OF CONTENTS	vi
LIST OF FIGURES	ix
LIST OF TABLES	xii
SYMBOLS	xiii
CHAPTER 1: INTRODUCTION	1
1.1 Introduction	1
1.2 Literature Reviews.....	2
1.3 Objectives.....	7
CHAPTER 2: BACKGROUND	8
2.1 Piezoelectricity.....	8
History of Piezoelectricity.....	8
Crystallography Applied to Piezoelectric Crystals.....	10
Piezoelectric Coefficient.....	15
Dielectric Materials.....	16
Electromechanical Coupling Coefficient.....	19
Electromechanical Coupling Coefficient Measurement.....	20
Resonance Method.....	22
2.2 Piezoelectric actuator and transducer.....	24
Single Layer Actuators.....	25
2-Layer Actuators.....	26
Multi-Layer Actuators.....	28
Actuators Performance.....	29
Series and Parallel Operation.....	30

TABLES OF CONTENTS (cont.)

2.3 Composite Materials.....	31
The 0-3 composite connectivity.....	31
2.4 Tape Casting Technique.....	32
2.5 Overall Properties of BaTiO ₃ and PVDF.....	33
CHAPTER 3: EXPERIMENTALS	38
3.1 Materials.....	31
3.2 Apparatus.....	31
3.3 Experimental Procedure.....	39
3.3.1 BaTiO ₃ -PVDF Composite Preparation.....	39
3.3.2 Physical Characterization.....	43
3.3.3 Electrical Characterization.....	44
OPEN Correction.....	45
SHORT Correction.....	46
Measurement Method.....	48
3.3.4 Electromechanical Characterization.....	48
3.3.5 Fabrication of Piezoelectric Stack.....	50
3.4 Finite Element Analysis.....	50
CHAPTER 4: RESULTS AND DISCUSSIONS	53
4.1 Physical Properties.....	53
4.2 Dielectric Properties.....	53
4.3 Electromechanical Property of the Piezoelectric Stack.....	55
CHAPTER 5: CONCLUSIONS	61
5.1 Main Conclusions.....	61
5.2 Suggestions and Further Investigations.....	62

TABLES OF CONTENTS (cont.)

BIBLIOGRAPHY	63
VITAE	70

LIST OF FIGURES

Figure 2.1	Classification of symmetry relating piezoelectric, pyroelectric and ferroelectric materials.	12
Figure 2.2	Schematic pictures of the (a) direct and (b) converse piezoelectric effects.	13
Figure 2.3	Concepts of single crystal and polycrystal.	14
Figure 2.4	A polarization process depicted for piezoelectric materials.	14
Figure 2.5	A parallel plate capacitor (a) without any dielectric, (b) filled with dielectric under short circuit condition and (c) filled with dielectric under open circuit condition.	17
Figure 2.6	The vector diagram of the permittivity.	18
Figure 2.7	(a) Parallel plate method and (b) related equations.	19
Figure 2.8	An original circuit for measuring the resonance of a piezoelectric material.	22
Figure 2.9	A constant voltage circuit for measuring the resonance of a piezoelectric material (T.P) (Piezoelectric Ceramic).	23
Figure 2.10	A constant current circuit for measuring the resonance of a piezoelectric material (T.P).	23
Figure 2.11	(a) Longitudinal, and (b) transverse single layer actuators.	26
Figure 2.12	2-layer transverse actuators expanding lengthwise.	27
Figure 2.13	Show several common bending configurations. The variety of mounting and motion options make benders a popular choice of design engineers.	27
Figure 2.14	Stack actuator.	28
Figure 2.15	Force vs. displacement diagram for a piezoelectric actuator.	30
Figure 2.16	A 2-layer bending actuators; Poled for Series (2-wire) and Parallel Operation (3-wire).	30
Figure 2.17	Schematic diagram showing the tape casting process.	33
Figure 2.18	A cubic perovskite unit cell showing the oxygen octahedral and the ionic positions for the A and B cations.	34

LIST OF FIGURES (cont.)

Figure 2.19	Unit cell distortions of BT single crystals; represents direction of dipole moment.	34
Figure 2.20	Approximate ion displacements in the cubic-tetragonal distortion in BT.	35
Figure 2.21	Unit cells of PVDF phases when project on a plan that perpendicular to the c axis; (a) α -phase, (b) β -phase, (c) γ -phase, and (d) δ -phase. When (o) and (O) represent carbon and fluorine atom, respectively (not show hydrogen atom).	36
Figure 2.22	(a) Schematic illustration showing random stacks of amorphous and crystal lamellae in PVDF polymer, (b) crystalline phase transformation due to mechanically stretching, and (c) crystalline orientation in PVDF under the applied high electric field.	36
Figure 2.23	Structure of β -phase PVDF.	37
Figure 3.1	Illustration of the apparatus necessary for the sample preparation.	40
Figure 3.2	Heat treatment conditions used in the composite sample preparation.	40
Figure 3.3	A glass plate of an area of $15 \times 15 \text{ cm}^2$ with a blade for tape casting.	41
Figure 3.4	Heat treatment conditions for an annealing process of the sample.	41
Figure 3.5	A corona poling setup. (a) The apparatus for the corona poling; (b) the details of the connected parts in (a).	42
Figure 3.6	The application of a DC electric field during the poling of the PVDF.	42
Figure 3.7	A schematic diagram of the preparation of the BT-PVDF composites.	43
Figure 3.8	Thickness gauge handling.	44
Figure 3.9	(a) HP 4263B LCR meter and (b) a test fixture 16451B.	44
Figure 3.10	(a) The attachment connected to the Guarded/Guard electrode for OPEN correction; (b) the details of the connected parts in (a).	45

LIST OF FIGURES (cont.)

Figure 3.11	Illustration of the messages appeared on the LCR meter display; (a) During the OPEN correction performance; (b) when the OPEN correction is complete.	46
Figure 3.12	(a) Connecting the attachment to the Unguarded electrode; (b) the details of the connected parts in (a).	47
Figure 3.13	Illustration of the messages appeared on the LCR meter display; (a) During the SHORT correction performance; (b) when the SHORT correction is complete.	48
Figure 3.14	A schematic diagram of a constant voltage circuit.	49
Figure 3.15	Experimental setup for the resonance measurement : (a) Function generator, (b) constant voltage circuit, (c) oscilloscope and (d) sample clamper.	49
Figure 3.16	The sketch of the 2-D stack.	51
Figure 4.1	Pictorial view of a composite tape (upper) which was cut into pieces with dimensions of about $10 \times 10 \text{ mm}^2$ (lower).	53
Figure 4.2	The experimental data of the (a) dielectric constant, and (b) dielectric loss as functions of frequency for the BT-PVDF composites.	54
Figure 4.3	Variations of the resonance and antiresonance of the composites with PVDF poled for a stack with (a) 1, (b) 2, (c) 3, and (d) 4 layers.	56
Figure 4.4	Changes in a resonance frequency as the layers of the stack increased.	57
Figure 4.5	Variations of the electromechanical coupling coefficient as a function of the number of the layers in the stack made from the samples with PVDF phased active.	58
Figure 4.6	Variations of the electromechanical coupling coefficient a function of number of layers in a stack made from the samples with both phases active.	59

LIST OF TABLES

Table 2.1	The crystallographic point groups arranged by crystal systems.	11
Table 2.2	The four piezoelectric coefficients (Moulson and Herbert, 1990).	15
Table 2.3	Typical vibration modes of piezoelectric materials.	21
Table 3.1	Material properties used in the FEA.	51
Table 4.1	Percentages of the difference (%diff) between experimental data (EXP) and FEA data for the stack of the BT-PVDF composites with PVDF poled.	57
Table 4.2	A summary of the properties of BaTiO ₃ , BT-PVDF, and PVDF materials.	60
Table 5.1	Physical and electromechanical properties of the BT-PVDF composites.	61
Table 5.2	The electromechanical coupling coefficient for all piezoelectric stacks.	62

SYMBOLS

A	Electrode area
C	Capacitance
D	Dielectric loss or dissipation factor
D	Electric displacement or at Electric displacement (superscript)
D_i	Electric displacement tensor
d	Piezoelectric coefficient
d_{ijk}	Piezoelectric coefficient tensor
E	Electric field
E_i	Electric field tensor
FEA	Finite element analysis
f_a	Antiresonance frequency
f_r	Resonance frequency
G	Gibbs function
j	Imaginary unit
k	Electromechanical coupling coefficient
k_{eff}	Effective electromechanical coupling coefficient
k_p	Electromechanical coupling coefficient in planar mode
k_T	Actuator stiffness
k_t	Electromechanical coupling coefficient in thickness mode
k_{15}	Electromechanical coupling coefficient in shear mode
k_{31}	Electromechanical coupling coefficient in transverse mode
k_{33}	Electromechanical coupling coefficient in longitudinal mode
M^C	Mass of ceramic
M^P	Mass of polymer
P	Polarization
S	Strain or at constant strain (superscript)
S_{ij}	Strain tensor
s	Elastic compliance
s_{ijkl}	Elastic compliance tensor

SYMBOLS

T_{ij}	Stress tensor
t	Thickness
ϵ_{ij}	Permittivity tensor
ϵ_0	Permittivity of free space
ϵ	Permittivity
ϵ'	Real part of permittivity
ϵ''	Imaginary part of permittivity
ϵ_r	Complex dielectric constant or complex relative permittivity
ϵ'_r	Dielectric constant or real part of complex relative permittivity
ϵ''_r	Imaginary part of complex relative permittivity
Θ	Temperature
χ	Electric susceptibility
Δt	Displacement
ρ	Density
ρ^c	Density of ceramic
ρ^p	Density of polymer
ϕ	Volume fraction of ceramic
σ	Conductivity
ω	Angular frequency

CHAPTER 1

INTRODUCTION

1.1 Introduction

For many decades, piezoelectric ceramics have been studied intensively in adaptive microelectromechanical systems (MEMs) such as sensors, transducers, micropositioners, and actuators. However, thin film technology has now been the basis of almost all modern high technology and plays an increasing role in the field with regard to many applications as: i) dielectrics for MLCC (Multilayer Layer Ceramic Capacitors) technology, ii) piezoelectric devices for microtransducers and frequency filters, iii) electronics for integrated ferroelectric devices, iv) FRAM (Ferroelectric Random Access Memory) etc. In comparison with ceramic pellets, multilayered structures have several advantages, such as small driving voltage, quick response, large generative force, and high electromechanical coupling (Uchino, 1997). During the entire service lifetime of piezoelectric devices, mechanical failure (e.g. cracking) often happened due to its brittleness and low fracture toughness. This is resulted from the microcrack growth which has been examined to be a major impediment to large scale usage (Li and Guo, 2007). Debonding along interfaces between electrodes and piezoelectric ceramics is experimentally shown to be the typical failure mode (Dos Santos e Lucato *et al.*, 2001; Koh *et al.*, 2004). Therefore, in an attempt to decrease the failure mechanism and avoid the catastrophic cracking failure of piezoelectric devices. It is desired to improve the mechanical property of piezoelectric ceramics.

Conventionally, materials like barium titanate (BaTiO_3 or BT), lead zirconate titanate ($\text{Pb}(\text{Zr},\text{Ti})\text{O}_3$ or PZT) and polyvinylidene fluoride (PVDF) polymer have been popular candidates for the use as piezo-materials (Patil, Ashwin and Radhakrishnan, 2007). Both BT and PZT ceramics display higher piezoelectricity than the PVDF polymer but the PZT, however, contains a harmful element (Pb) for the environment. PVDF is being received wide attention today in various fields due to

the ease of processing, its flexibility, low density, low acoustic and mechanical impedance (Harrison and Ounaies, 2001).

This work proposes the piezoelectric composites which are able to produce by mixing the BT particles which is non-toxic with the PVDF-polymer host. A shape forming used in this work is a tape casting method. The material is anticipated to give advantages of mechanical flexibility and retain useful piezoelectric properties. The layers of the material are further formed into a stack similar to conventional transducers available in sectorial markets. Two ways used in this work to study the electromechanical properties of the piezoelectric stacks of the BT and the PVDF are experimental procedure and a finite element analysis (FEA).

1.2 Literature Reviews

Piezoelectricity was first observed in 1880 and this property has been investigated in many types of materials ever since. A historical review of these measurements and some of theoretical principle of this effect clearly show that piezoelectricity has continued to interest and puzzle the investigators for over a century. Newnham, Skinner and Cross (1978) were probably the first to propose the possibility of a piezo-and pyroelectricity in ceramic-polymer composites. They found that the connectivity is a critical parameter in composites design to use as piezoelectric transducers or as pyroelectric detectors. There are 10 important connectivity patterns in diphasic solids, ranging from 0-0 unconnected checkerboard pattern to 3-3 pattern in which phases 3-dimensionally self-connected. Their series and parallel models for piezoelectric and pyroelectric composite lead to several interesting results, such as a diphasic pyroelectric in which neither phase is pyroelectric. The models are also helpful in interpreting the structure-property relations in single-phase material where the crystal structures mimic certain connectivity pattern.

In 1989, Smith found that combining a piezoelectric ceramic and a passive polymer to form a piezocomposite allowed the transducer engineers to design new piezoelectrics that offer substantial advantages over the conventional

piezoelectric ceramic and polymer. The rod composite geometry provided materials with enhanced electromechanical coupling and with acoustic impedance closely related to that of tissue; these advantages made transducers capable for medical ultrasonic imaging with high sensitivity and compact impulse response (Smith, 1989).

A few years later, Smith studied a simple physical model of 1-3 piezoelectric composites. The advantages of the material properties related to their thickness-mode oscillation. Expressions were derived for the composite's material parameters in terms of the volume fraction of piezoelectric ceramic and properties of the constituent piezoelectric ceramic and passive polymer. This model illustrated that the composite structure enhanced its hydrostatic charge coefficient (d_h), hydrostatic voltage coefficient (g_h), and hydrostatic coupling factor (k_h) (Smith, 1993).

Dias and Das-Gupta (1994) presented the piezo-and pyroelectric properties of composites with 0-3 connectivity type. A review of the electroactive properties predicting model of 0-3 composites was presented together with a proposal for a new mixed connectivity cubes model to be applicable in the case of high ceramic loading and/or when the ceramic grain size incorporated in the polymer matrix was comparable to the thickness of the sample. They also presented the experimental results of the piezo-and pyroelectric properties of various ferroelectric composite materials.

Kwok, Chan, and Choy (1994) fabricated 1-3 composites of PZT in the copolymer of the PVDF, i.e., P(VDF-TrFE) by embedding pre-sintered PZT rods in a pre-poled copolymer matrix. Their observations have been summarized as:

1. The characteristic resonance of the individual PZT rods were clearly observed. The copolymer matrix did not significantly modify the characteristic resonance of the individual PZT rods, because the soft copolymer matrix did not impose an appreciable clamping on the rods.
2. The thickness resonance of the poled copolymer matrix was very weak and, in the sample geometry, merged with the PZT resonance to form a broad resonance peak.
3. The resonance characteristics of the composites with PZT and copolymer poled in the same and opposite directions were quite similar. Higher

electromechanical coupling constant (k_t) is obtained if the two phases were poled in the same direction.

4. The radial mode resonance of the 1-3 composites depended only on the diameter of the sample but did not depend on sample poling history.

Kwok, Chan and Choy have also evaluated the elastic, dielectric and piezoelectric constants using five different methods: 1) the IEEE Std. 176 method, 2) the method of Smits, the method of Sherrit (Sherrit, Wiederick, and Mukherjee, 1992), 3) a software package “Piezoelectric Resonance Analysis Program (PRAP)”, and 4) a nonlinear regression method. The IEEE Std. 176 method was strictly valid only for lossless materials. They have found that it was applicable to material with moderate loss, in agreement with experimental results. However, for high-loss materials such as PVDF, the k_t value evaluated using this method was much higher than the value determined by the nonlinear regression method.

In 1999, Chan, Ng and Choy fabricated 0-3 composite PZT/P(VDF-TrFE) by incorporating PZT powder into a P(VDF-TrFE)copolymer matrix. In this work, original experimental results on the properties of 0-3 composite PZT/P(VDF-TrFE) poled under different condition were reported and possible reasons behind the reinforcement and cancellation of piezoelectric and pyroelectric properties were explained. The changes in the pyroelectric and piezoelectric coefficients of the poled 0-3 composites PT/P(VDF-TrFE) with increasing ceramic volume fraction could be described by modified linear mixture rules (Chan, Ng and Choy, 1999). Lau *et al.* (1999) measured the piezoelectric coefficient of the 0-3 composite PZT/P(VDF-TrFE) using a laser interferometric technique. The diphasic composites which were poled oppositely is able to enhance the piezoelectric activity as a whole.

In 2000, Ng *et al.* showed that the pyroelectric activities of the 0-3 composite PZT/P (VDF-TrFE) would reinforce and the piezoelectric activities would partially cancel if the ceramic and copolymer phases were poled in the same direction. On the other hand, when the ceramic and copolymer phases were poled in opposite directions, their piezoelectric would reinforce while their pyroelectric activities would partially cancel. Im *et al.* (2000) simultaneously fabricated multilayer piezoelectric actuators (MPAs) by using a 70Ag/30Pd paste as internal electrodes because of its

low cost and low sintering temperature. The MPAs with 75 layers were fabricated with layer thicknesses of 30 ± 35 nm. It was clearly showed that the 70Ag/30Pd paste electrodes had a good matchability with PNN±PT±PZ ceramics, cofired at 1,050 °C for 3 h since no defects such as delamination of ceramic layers, diffusion of internal electrode into ceramic body, shortage of internal electrode and gapping phenomena were detected. The MPA exhibited maximum displacement of ~4 mm at 2.85 kV/mm, superior to other products. The dissipation factor of the MPA was below 3%, applicable to practical uses due to low heat generation. Therefore, it was confirmed that the MPA having a low cost and a good electrical property can be mass-produced using a AgPd internal electrode.

Burianova and Prokopova observed piezoelectric coefficient of PZT ceramic and the ceramic-polymer 0-3 composites by resonance and laser interferometric methods. The obtained results d_{33} coefficients by the both methods were in good agreement (Burianova and Prokopova, 2001). Ng *et al.* (2000) showed that 0-3 composites of lead zirconate titanate particles dispersed in a polyvinylidene fluoridetrifluoroethylene copolymer matrix may have a good potential for pyroelectric sensor applications.

In 2002, Wang *et al.* studied the characteristics of the multilayer actuators. They are recognized as being the best pre-clinical assessment of a hearing implant. They give a very satisfactory performance over the audio frequency range, with high signal fidelity and adequate stapes movement at relatively low power consumption. The power consumption of 0.7 mW per volt of excitation at 1 kHz is low enough for it to be used in a partially implantable hearing aid. This power source could be provided externally via a percutaneous coupling. It generates considerably more driving force than a bimorph actuator. The simulated surgical implantation showed that the procedure is straightforward. Improved methods for anchoring the actuator and coupling it to the incuses are currently being developed.

In 2003, Kondo *et al.* fabricated of $\text{PbNi}_{1/3}\text{Nb}_{2/3}\text{O}_3\text{-PbTiO}_3\text{-PbZrO}_3$ (PNiNb-PT-PZ) multilayer ceramic actuators with silver internal electrodes sintered at 900 °C. They investigated the influence of the excess lead oxide (PbO) content on the sinterability of the PNiNb-PT-PZ ceramic. A liquid phase was formed by adding

the excess PbO, and the liquid phase promoted the sintering of the ceramic. As a result, the sintering temperature could be decreased to around 900 °C with 1 mol% of excess PbO. The multilayer actuator was fabricated by co-firing the PbO-rich PNiNb–PT–PZ ceramic and the silver internal electrodes. The displacement of this actuator was the same as that of an actuator fabricated with stoichiometric ceramic powder sintered at 1,050 °C and silver–palladium alloy electrodes. The displacement of the actuator with silver electrodes did not decrease after it had been driven for 9.65 days in an environment at 40 °C with humidity of 90%. The PNiNb–PT–PZ ceramic is thus promising as a piezoelectric material that can be sintered at a low temperature and used in multilayer actuators with silver internal electrodes.

The piezoelectricity and polarization of multilayer actuators, being designed to stack ceramic layer and electrode layer alternately, were investigated under a consideration of geometry, the thickness ratio of the ceramic layer to electrode layer. The actuators were fabricated by tape-casting of $0.42\text{PbTiO}_3\text{--}0.38\text{PbZrO}_3\text{--}0.2\text{Pb}(\text{Mn}_{1/3}\text{Nb}_{2/3})\text{O}_3$ followed by laminating, burn-out and co-firing process. Increase in polarization and electric field-displacement with thickness of the ceramic layer was attributed to the change of non-180/180° domain ratio. The relative amount of non-180° domain reorientation observed from the XRD diffraction indicates that the internal stress is generated between the two layers in a manner that the ceramic tends to contract along X_3 axis and to elongate along X_1 axis. In addition, the piezoelectricity and actuation behaviors were found to depend upon the volume ratio (or thickness ratio) of ceramic layer to total layer. The 60 μm -thick ceramic layer actuator showed lower dependence of dielectric polarization and permittivity and piezoelectric coefficient on electric field than a 120 μm -thick actuator. The change in dielectric and piezoelectric properties may be caused by the retardation of non-180 domain wall motion due to the internal stress generated between the two layers (Jeong *et al.*, 2004).

In 2008, a large-area multilayer ceramic actuator with a width/thickness ratio of 30 was fabricated without bending or wrenching by co-firing of piezoelectrically active PZN-PZT layers and silver metal layers prepared by tape-casting method. The thickness of the piezoelectric and electrode layers was about 120

and 20 mm, respectively. The sintered tape showed the highest density at a powder/(binder + plasticizer) wt. ratio of 10.8. A silver inner-electrode containing 30% of PZN-PZT ceramic frits was effective for the preparation of multilayer ceramic actuator, with no reaction being observed between PZN-PZT and silver interface. The multilayer PZN-PZT/Ag actuator showed a piezoelectric strain of 0.34% compared to 0.38% for the single-layer bulk specimen. The voltage required to obtain a strain of 0.3% was decreased from 2500 to 260 V for the actuator with 13 layers (Choi *et al.*, 2008).

1.3 Objectives

The objectives of this work are:

1. Prepare the composite materials of BT ceramic and PVDF polymer and form the material into a thick layer by a tape-casting method.
2. Study the dielectric properties of the prepared composites under different poling condition.
3. Form a piezoelectric stack from the layers of the prepared composites and study their electromechanical properties using a resonance method and a finite element analysis.

CHAPTER 2

BACKGROUND

This chapter gives the overviews of the piezoelectricity, piezoelectric stacking transducers, patterns of composite connectivity, tape casting technique, and the overall properties of the ceramic and polymer phases (BT and PVDF, respectively) of the BT-PVDF composites.

2.1 Piezoelectricity

History of Piezoelectricity

The first experimental demonstration of a connection between macroscopic piezoelectric phenomena and crystallographic structure was published in 1880 by Pierre and Jacques Curie. Their conclusive experiment is to measure the surface charges appearing on specially prepared crystals (tourmaline, quartz, topaz, cane sugar and Rochelle salt) which were subjected to an external mechanical stress. This is namely the direct piezoelectric effect. However, the Curie brothers did not predict that crystals also exhibited the converse piezoelectric effect (stress in response to applied electric field). This property was mathematically deduced from fundamental thermodynamic principles by Lippmann in 1881. A year later, the Curies immediately confirmed the existence of the "converse effect". It was not until the experiments by Neumann in 1890, that he established the existence of three basic principles that appears to govern the physical behavior of all crystalline materials (Ballato, 1996). Neumann suggested that:

1. The symmetry elements for any physical property of a crystal must include all symmetry elements of the point group of that crystal.
2. Every physical property of a crystal must possess at least the symmetry of the point group of that crystal.

3. Any kind of symmetry that is possessed by the crystallographic form of a material is also possessed by the material in respect of every physical property it possesses.

In 1893, Lord Kelvin provided the real groundwork for understanding the piezoelectric concept when he developed models which explained and expanded the concept of the macroscopic/phenomenological theory of piezoelectricity, based on thermodynamic principles. It was not until the work of Voigt in 1894, that equations governing the linear behavior of piezoelectric crystals were described as "tensors". This "Tensor concept" suggested that "Stress (T) is proportional to Strain (S) which is proportional to electric field". Therefore, the piezoelectric coefficient which couples both "mechanical and electrical tensor variables" is the same (Ballato, 1996). The state of piezoelectric knowledge was summarized in Voigt's "Lerbuch der Kristallphysik" was published and became a standard reference work detailing the complex electromechanical relationships in piezoelectric crystals (Cady, 1964).

The first major practical application of piezoelectric materials came in the World War I. In 1917, Langevin and co-workers (Langevin *et al.*, 1950) developed a piezoelectric ultrasonic transducer (quartz crystal) during World War I. Their success opened up opportunities for piezoelectric materials in underwater applications as well as a host of other applications such as ultrasonic transducers, microphones, loudspeakers, accelerometers, bender element actuators, phonograph pick-ups, signal filters, etc. And 18 years later, Busch and Scherrer discovered piezoelectricity in potassium dihydrogen phosphate (KDP). The KDP family was the first major family of piezoelectrics and ferroelectrics to be discovered.

During World War II, research in piezoelectric materials expanded to the U.S., the Soviet Union and Japan. Up until then, limited performance by these materials inhibited commercialization but that changed when a major breakthrough came with the discovery of barium titanate and lead zirconate titanate in the 1940s and 1950s respectively. These families of piezoelectric ceramics exhibited very high dielectric and piezoelectric properties. Furthermore, they offered the possibility of tailoring their behavior to specific responses and applications by the use of dopants

(Jordan and Ounaies, 2001). A decade later, researchers had discovered a weak piezoelectric effect in whale bone and tendon. This began an intense search for other organic materials that might exhibit piezoelectricity. In 1969, Kawai found very high piezo-activity in the polarized fluoropolymer, polyvinylidene fluoride (PVDF). While other materials, like nylon and PVC exhibit the effect, none are as highly piezoelectric as PVDF and its copolymers (Kawai, 1969). Their characteristics are lightweight, tough, readily manufactured into large areas, and can be cut and formed into complex shapes. This precipitated further works and led to a greater understanding structures and behaviors of piezoelectrics. Extensive researches and developments throughout the last five decades has led to the use of piezoelectrics in a wide variety of commercial, communications, automotive field, medical, and military applications (Jordan and Ounaies, 2001).

To date, it is desired to use lead-free materials for environmental protection. For example, the legislation will be enforced in the EU as the draft directives on waste from electrical and electronic equipment (WEEE), restriction of hazardous substances (RoHS) and end-of life vehicles (ELV). Therefore, lead-free piezoelectric materials have been widely attracting attention as new materials in place of PZT ceramics.

Crystallography Applied to Piezoelectric Crystals

Generally, most piezoelectric materials of interest for technological applications are crystalline solids. These can be single crystals, either formed in nature or formed by synthetic processes, or polycrystalline materials like ferroelectric ceramics which can be rendered piezoelectric and given, on a macroscopic scale, a single-crystal symmetry by the process of poling. Depending on their degrees of symmetry, crystals are commonly classified into 7 systems: triclinic (the least symmetrical), monoclinic, orthorhombic, tetragonal, trigonal, hexagonal, and cubic. The systems, in turn, are divided into point groups (classes) according to their symmetry with respect to a point. Table 2.1 provides the detail of these point groups arranged by seven crystal systems (IEEE Std 176, 1988).

Table 2.1 The crystallographic point groups arranged by crystal systems (Lang *et al.*, 2001).

Crystal system	International Point Groups	Pyroelectric	Piezoelectric	Centrosymmetry
Triclinic	1	√	√	
	$\bar{1}$			√
Monoclinic	2	√	√	
	<i>m</i>	√	√	
	$2/m$			√
Orthorhombic	222		√	
	<i>mm</i> 2	√	√	
	<i>mmm</i>			√
Tetragonal	4	√	√	
	$\bar{4}$		√	
	$4/m$			√
	422		√	
	$4mm$	√	√	
	$\bar{4}2m$		√	
	$4/m\ mm$			√
Trigonal	3	√	√	
	$\bar{3}$			√
	32		√	
	$3m$	√	√	
	$\bar{3}m$			√
Hexagonal	6	√	√	
	$\bar{6}$		√	
	$6/m$			√
	622		√	
	$6mm$	√	√	
	$\bar{6}m2$		√	
	$6/m\ mm$			
Cubic	23		√	
	$m\bar{3}$			√
	432			
	$\bar{4}3m$		√	
	$m\bar{3}m$			√

There are 32 classes, 11 of these classes have a centre of symmetry. The remaining 21 non-centrosymmetric classes, and the 20 crystal classes (excepted 432 crystal class) are known to be piezoelectric, i.e., show changes in their internal polarization for change in mechanical stress and the converse effect also holds. Ten of these twenty classes have a unique polar axis and they possess spontaneous polarization (i.e., electric dipole moment per unit volume). Their spontaneous polarization is decreased by increasing of temperature. Thus these materials are named pyroelectric. Ferroelectric are subclass of the pyroelectrics, which has two or more orientation stages (in the absence of an externally impressed electric field), which can be switched from one state to another by an electric field. These two orientational states have identical crystal structure, but differ only in their electric polarization vectors at zero electric field. All ferroelectric materials are piezoelectric material, but not piezoelectric materials are ferroelectric material. However, the converse is not true, i.e., all piezoelectrics are not pyroelectric and all pyroelectrics are not ferroelectric, as illustrated in Figure 2.1

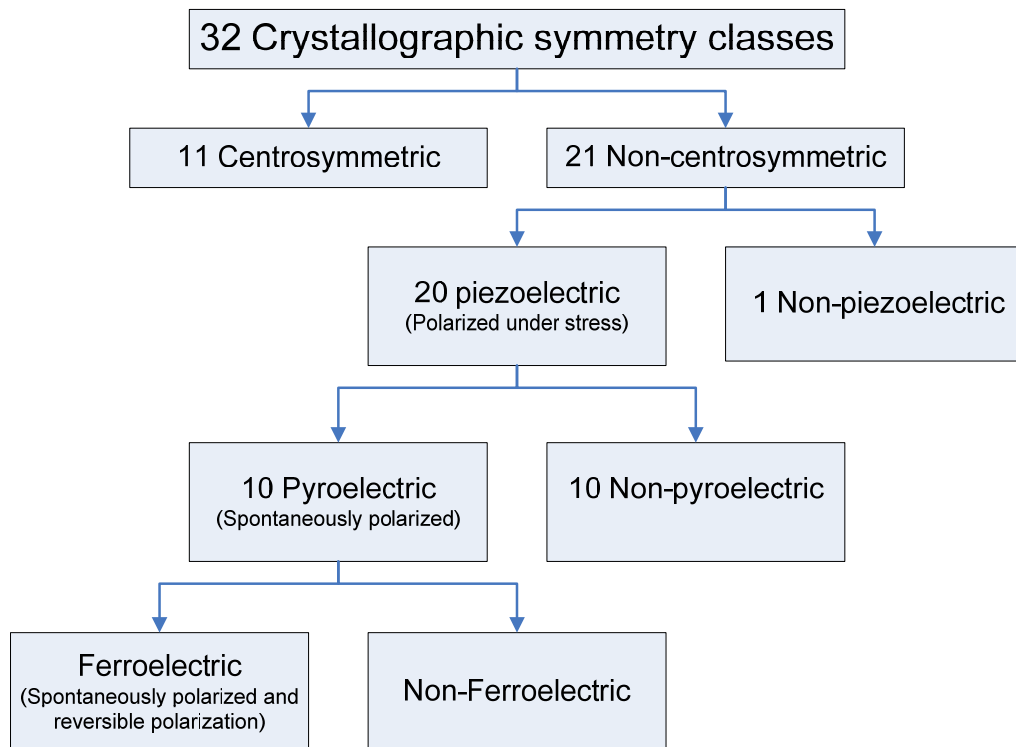


Figure 2.1 Classification of symmetry relating piezoelectric, pyroelectric and ferroelectric materials (Lang *et al.*, 2000).

Piezoelectric materials are a type of dielectric crystal that produces an electric charge when a mechanical stress is applied. This effect is referred to as “*the direct piezoelectric effect*”. Conversely, a mechanical deformation is produced under an electric field is called “*the converse piezoelectric effect*”. The effects were schematically shown in Figure 2.2.

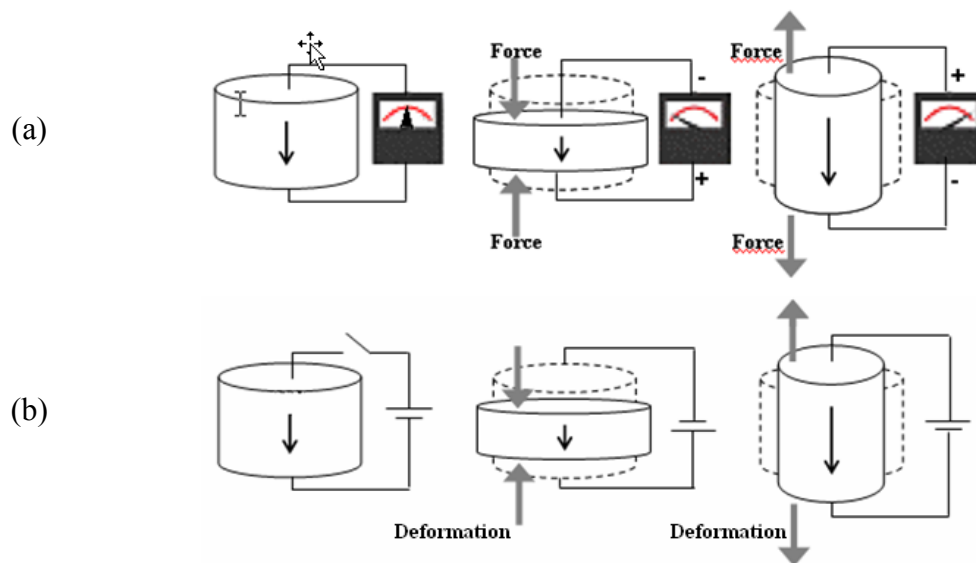


Figure 2.2 Schematic pictures of the (a) direct and (b) converse piezoelectric effects.

Normally, 2 types of piezoelectric effect are formed in dielectric crystals which have no a center of symmetry. These materials can have single crystal structure and polycrystalline structure (Figure 2.3). To explain these (IEEE Std 176, 1988), crystals are considered as being composed of molecules with a polarization, one end is more negatively charged and the other end is positively charged, and is called a dipole. The polar axis is an imaginary line that runs through the center of both charges on the molecule. In a single crystal, the polar axes of all of the dipoles lie in one direction. On the part of a polycrystal, there are different regions within the material that have a different polar axis or dipoles are oriented at random in which it exhibits a weak piezoelectric property. Polycrystalline structure can be given single crystal symmetry by the process of poling as depicted in Figure 2.4.

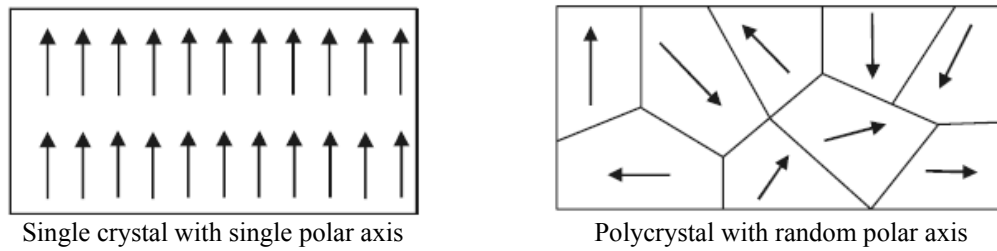


Figure 2.3 Concepts of single crystal and polycrystal.

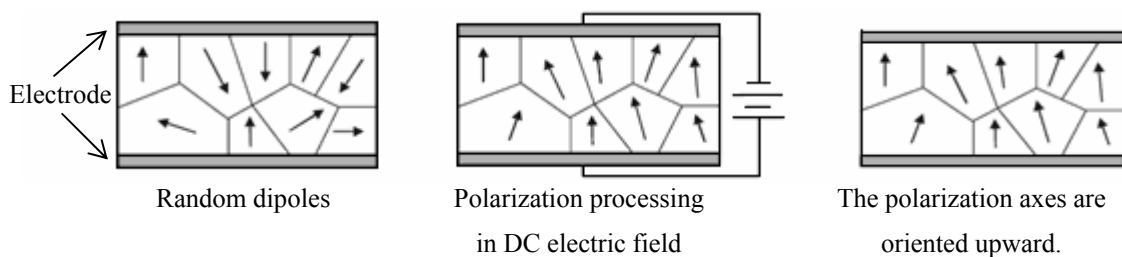


Figure 2.4 A polarization process depicted for piezoelectric materials.

Poling is a process by which a DC electric field is applied to a specimen of multi-domain crystal to switch the direction of electric dipoles. An electric field of the order of kV/mm is applied to the crystal to align the internal electrical dipoles in a single orientation. Due to the strong dielectric property of the crystal, the electric dipole moment remains unchanged after the electric field is removed, and the crystal thus exhibits a strong piezoelectric property

In order to describe behaviors of the coupled system in piezoelectric media, let us consider single crystal is based on the linear interaction processes between electrical and mechanical systems and the adiabatic and isothermal conditions are assumed. The constitutive equations can be derived Legendre transformations of the thermodynamic functions or energy density which is a quadratic form in electromechanical state systems such as Helmholtz Free Energy, Gibbs Free Energy, Elastic Gibbs Energy and Electric Gibbs Energy (Ikeda, 1990). The choice of the thermodynamical function leads to different variable-type relations (different forms). The constitutive relations are given by

d -form:

$$S_{ij} = \frac{\partial G}{\partial S} = s_{ijkl}^E T_{kl} + d_{kij} E_k \quad (2.4)$$

$$D_i = \frac{\partial G}{\partial E} = d_{ikl} T_{kl} + \varepsilon_{ik}^T E_k \quad (2.5)$$

which is characterized by “complementary energy function or Gibbs function (G)”.

$$G(T, E) = \frac{1}{2} s_{ijkl}^E T_{ij} T_{kl} + d_{kij} E_k T_{ij} + \frac{1}{2} \varepsilon_{ij}^T E_i E_j \quad (2.6)$$

where the subscripts are $i, j, k, l=1$ to 3 .

Piezoelectric Coefficient

In piezoelectric materials, the various piezoelectric coefficients of each forms are properly defined by the following partial derivatives, where the subscripts indicate the variables held constant (Θ is the temperature).

Table 2.2 The four piezoelectric coefficients (Moulson and Herbert, 1990).

Forms	Effects	Piezoelectric Coefficients
d	Direct	$d = \left(\frac{\partial D}{\partial T} \right)_{E, \Theta}$
	Converse	$d = \left(\frac{\partial S}{\partial E} \right)_{T, \Theta}$
g	Direct	$g = - \left(\frac{\partial E}{\partial T} \right)_{D, \Theta}$
	Converse	$g = - \left(\frac{\partial S}{\partial D} \right)_{T, \Theta}$
e	Direct	$e = \left(\frac{\partial D}{\partial S} \right)_{E, \Theta}$
	Converse	$e = - \left(\frac{\partial T}{\partial E} \right)_{S, \Theta}$
h	Direct	$h = - \left(\frac{\partial E}{\partial S} \right)_{D, \Theta}$
	Converse	$h = - \left(\frac{\partial T}{\partial D} \right)_{S, \Theta}$

Dielectric Material

When an electric field is applied on a particular material, no current flows within the material because there are no free charged particles within the material to conduct the current. These materials are dielectrics and are commonly known as insulators. Although dielectrics do not conduct current, they may be polarized under the influence of an externally applied electric field. Within dielectrics, there are bound charges arising from the simple fact that all matter consist subatomic charged particles (i.e. protons and electrons). Some dielectrics are made of polar molecules in which, due to the geometry, one end of the molecule has a slightly more positive charge whereas the other end has a slightly more negative charge even though the whole molecule is neutral. Such molecules possess a dipole moment and are also known as electric dipoles. However, since the molecules are randomly oriented in the material, macroscopically the material is also neutral. But when an external electric field is applied, all polar molecules will align themselves in the direction of the field and the material is said to be polarized. For dielectrics that are composed of non-polar molecules, there are no intrinsic dipole moments. But the application of an external electric field modifies the distribution of charges in each molecule such that dipole moments are induced. In other words, whether the molecules are polar or non-polar, the presence of an external field will polarize the material by aligning the electric dipoles. The volume density of the electric dipole moment is defined as the polarization, P and the overall charge neutrality of dielectrics in an external field is described (William and Callister, 2005) by

$$D = \epsilon_0 E + P \quad (2.19)$$

The vacuum contribution caused by the externally applied electric field is represented by the term $\epsilon_0 E$, and the electrical polarization of the dielectrics in the system is described by P . This relation is independent of the nature of the polarization which could be pyroelectric polarization, by piezoelectric polarization or dielectric polarization (by an external electric field, E).

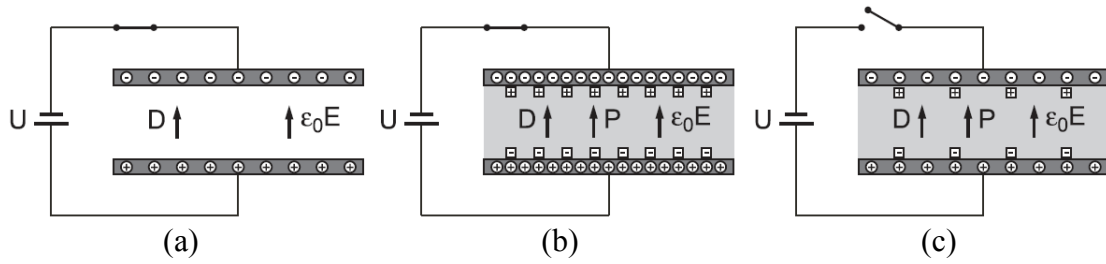


Figure 2.5 A parallel plate capacitor (a) without any dielectric, (b) filled with dielectric under short circuit condition and (c) filled with dielectric under open circuit condition.

Considering a simple parallel plate capacitor filled with dielectric (Figure 2.5), 2 cases have to be distinguished. If the applied voltage is kept constant ($E = \text{constant}$ short circuit condition), additional free charges need to flow into the system to increase D . If the charges on the plates are kept constant ($D = \text{constant}$ open circuit condition), the field E and the voltage between the plates will therefore decrease according to Equation (2.19). For many dielectric materials, P is proportion to the electric field in a linear approximation (William and Callister, 2005) by

$$P = \varepsilon_0 \chi E \quad \text{or} \quad D = \varepsilon_0 \varepsilon_r E = \varepsilon E \quad (2.20)$$

where the electric susceptibility, χ is related to the dielectric constant or relative permittivity (ε_r) by $\chi = \varepsilon_r - 1$. ε and ε_0 are the permittivity of the material and free space ($8.854 \times 10^{-12} \text{ F/m}$), respectively.

Dielectric constant (ε_r) is relative to the permittivity of free space (ε_0). The real part of complex relative permittivity (ε_r') is a measure of how much energy from an external field is stored in a material. For most solids and liquids are $\varepsilon_r' > 1$. The imaginary part of complex relative permittivity (ε_r'') is called the loss factor and is a measure of how dissipative or lossy a material is to an external field. ε_r'' is always > 0 and is usually much smaller than ε_r' . The loss factor includes the effects of both dielectric loss and conductivity. When complex permittivity is drawn

as a simple vector diagram as shown in Figure 2.6, the permittivity of material (ϵ) can be mathematically expressed by a complex dielectric permittivity (Sadiku, 1995):

$$\epsilon = \epsilon_0 \epsilon_r = \epsilon' - j\epsilon'' \quad (2.21)$$

or

$$\epsilon_r = \frac{\epsilon'}{\epsilon_0} - j \frac{\epsilon''}{\epsilon_0} = \epsilon'_r - j\epsilon''_r \quad (2.22)$$

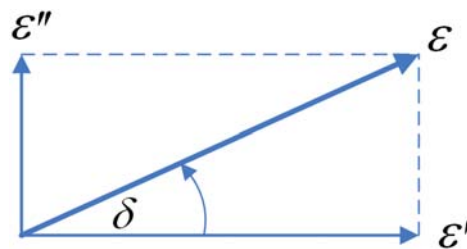


Figure 2.6 The vector diagram of the permittivity.

Constant ϵ , ϵ_0 , ϵ'_r , and ϵ''_r have the same meaning as before, while j is the imaginary unit. ϵ' and ϵ'' are the real and imaginary parts of permittivity and both parts are related to the stored energy and dissipation (or loss) of energy within the material. The real and imaginary components are 90° out of phase. The vector sum forms an angle δ with the real axis. The tangent of this angle, $\tan \delta$ or loss tangent or dissipation factor (D) is usually expressed (Sadiku, 1995; Agilent Application Note 1369-1, 2006) as

$$D = \tan \delta = \frac{\epsilon''}{\epsilon'} = \frac{\epsilon''_r}{\epsilon'_r} = \frac{\sigma}{\omega \epsilon'} \quad (2.23)$$

where σ is the conductivity of the material in mhos per meter or siemens per meter and ω is known as the angular frequency in radians per second.

Practically, the parallel plate method involves sandwiching a thin sheet of material or liquid between two electrodes to form a capacitor (Figure 2.7). The measured capacitance is then used to calculate permittivity. In an actual test setup, two electrodes are configured with a test fixture sandwiching the dielectric material.

The impedance-measuring instrument would measure vector components of capacitance (C) and dissipation (D). The real part of the relative permittivity can be calculated by using Equation (2.24) (Agilent Application Note 1369-1, 2006):

$$\epsilon'_r = \frac{\epsilon'}{\epsilon_0} = \frac{tC_p}{\epsilon_0 A} \quad (2.24)$$

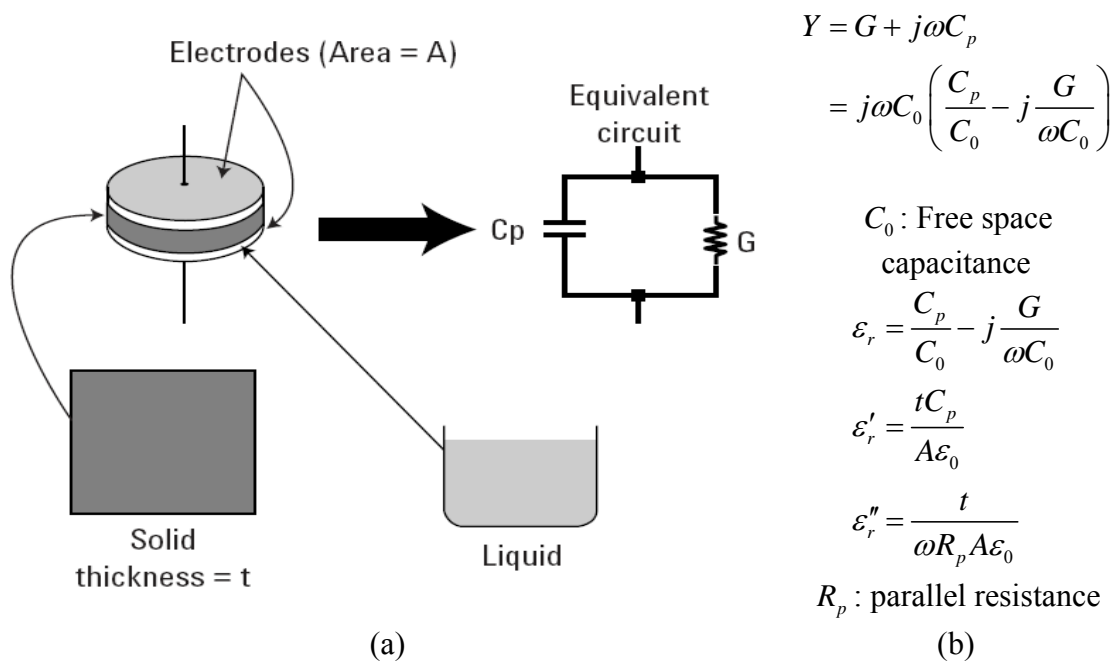


Figure 2.7 (a) Parallel plate method and (b) related equations (Agilent Application Note 1369-1, 2006).

Electromechanical Coupling Coefficient

The electromechanical coupling coefficient, k -value, is the efficiency of converting electrical energy into mechanical energy, or converting mechanical energy into electrical energy. The k -value defined in terms of by k^2

$$k^2 = \frac{w_1}{w_2} \quad (2.25)$$

For the direct effect, w_1 and w_2 are the mechanical energy output and electrical energy input, respectively. On the other hand, for the converse effect, w_1 and w_2 are the electrical energy output and the mechanical energy input, respectively. Since piezoelectricity is a linear interaction between electrical and mechanical systems, the electromechanical coupling coefficient can be defined by following Equation (2.26) (Ikeda, 1990).

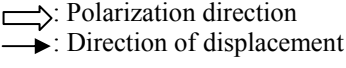
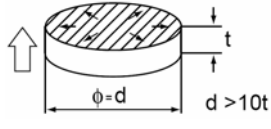
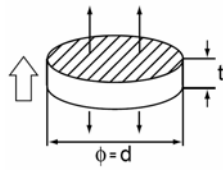
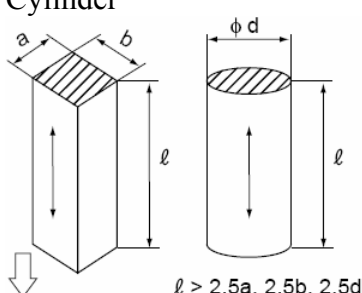
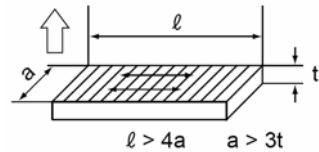
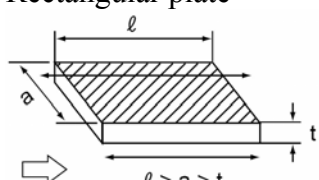
$$k^2 = \frac{d^2}{\varepsilon^T s^E} \quad (2.26)$$

where d , ε^T and s^E are the piezoelectric constant, dielectric constant at constant stress and elastic compliance at constant electric field, respectively.

Electromechanical Coupling Coefficient Measurement

The electromechanical coupling coefficient, k can be calculated for the various modes of vibration investigated by one of the two following methods. First, the static method is the original measurement using the direct effect. In details, putting a weight on a material and observing the charge generated by charge detector such as an electrometer. This method is rather indeterminate since they may depend on how much of the charge generated has leaked off during the measurement. The second method is the dynamic or resonance method. It is an easy and accurate method for evaluating the k -value by measuring the resonance and anti-resonance frequencies which relate to the k -value (Mason and Jaffee, 1954). In this method, if an AC voltage of varying frequency is applied to a piezoelectric ceramic of a certain shape (as listed in Table 2.3), there is a specific frequency at which the ceramic produces a very strong vibration. This frequency is called the resonance frequency which depend on the shape, orientation of polarization, and the direction of the electric field. Each vibration mode has unique resonance, f_r (the impedance is at a minimum) and anti-resonance f_a (oppositely, the impedance is at a maximum).

Table 2.3 Typical vibration modes of piezoelectric materials.

Mode of Vibration	Shape 	Electromechanical Coupling Coefficient
Radial	Disk 	$k_p^2 \cong \left(2.51 \cdot \frac{f_a - f_r}{f_a} \right) - \left(\frac{f_a - f_r}{f_a} \right)^2$
Thickness extension	Disk 	$k_t^2 = \frac{\pi}{2} \cdot \frac{f_r}{f_a} \cot \left(\frac{\pi}{2} \cdot \frac{f_r}{f_a} \right)$
Longitudinal length	Cylinder 	$k_{33}^2 = \frac{\pi}{2} \cdot \frac{f_r}{f_a} \cot \left(\frac{\pi}{2} \cdot \frac{f_r}{f_a} \right)$
Transverse length	Rectangular plate 	$\frac{k_{31}^2}{1 - k_{31}^2} = - \frac{\pi}{2} \cdot \frac{f_a}{f_r} \cot \left(\frac{\pi}{2} \cdot \frac{f_a}{f_r} \right)$
Thickness shear	Rectangular plate 	$k_{15}^2 = \frac{\pi}{2} \cdot \frac{f_r}{f_a} \cot \left(\frac{\pi}{2} \cdot \frac{f_r}{f_a} \right)$

(PIEZOTITE[®], 2008; Ferroperm Piezoceramics, 2003).

The effective electromechanical coupling, k_{eff} is also frequently used to express the electromechanical coupling of an arbitrary resonator regardless of its shape as given by:

$$k_{eff}^2 = \frac{f_a^2 - f_r^2}{f_r^2} \quad (2.27)$$

Resonance Method

A popular method for evaluating the electromechanical coupling coefficient value of piezoelectric materials is the resonance method, because it does not have any problem with the electric charge leakage during the experiment. The resonance method can determine the electromechanical coupling coefficient value from the resonance characteristics of the piezoelectric material. As mentioned earlier, the f_r is where the piezoelectric material's impedance is at a minimum while the current is at a maximum. Oppositely, the f_a corresponds to the frequency at the lowest current value and at the highest impedance. An original circuit for measuring the resonance and anti-resonance frequencies of the piezoelectric material is shown in Figure 2.8

In practice the electronic circuits were developed for measuring the resonance. Some circuits were shown in Figures 2.9 and 2.10.

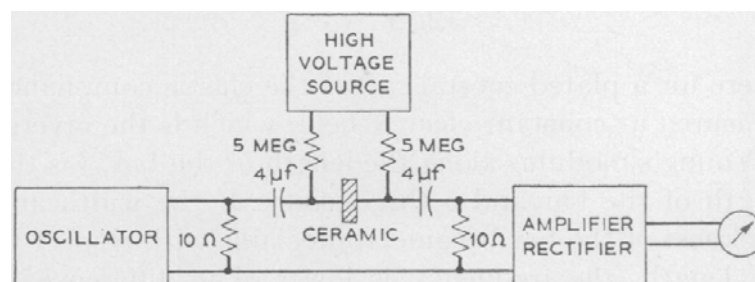


Figure 2.8 An original circuit for measuring the resonance of a piezoelectric material (Mason and Jaffee, 1954).

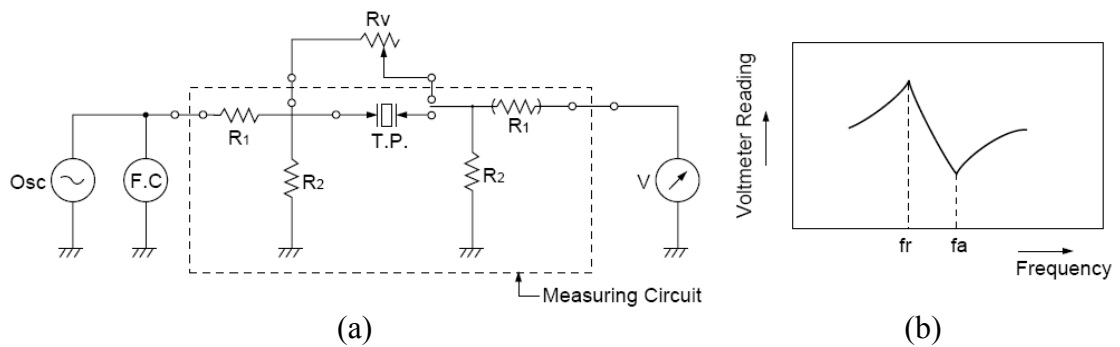


Figure 2.9 A constant voltage circuit for measuring the resonance of a piezoelectric material (T.P) (PIEZOTITE[®], 2008).

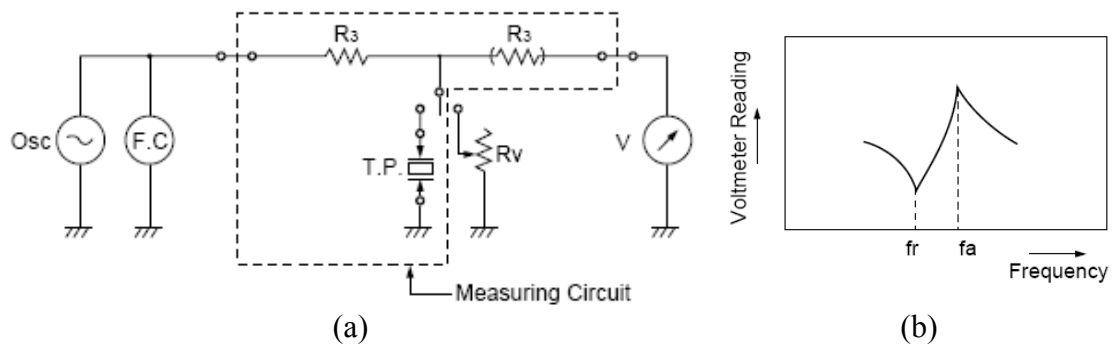


Figure 2.10 A constant current circuit for measuring the resonance of a piezoelectric material (T.P) (PIEZOTITE[®], 2008).

The constant voltage circuit includes an oscillator (osc) for generating an AC-voltage and the input resistors R_1 and R_2 are used to apply a constant voltage signal to the piezoelectric material. The current is passing through the piezoelectric material. If the piezoelectric material's impedance is much greater than R_2 , the output voltage, which is across the output resistor R_2 , is proportional to the piezoelectric material's admittance. The frequency where the output voltage is maximized is the resonance frequency (f_r) and the frequency where the output voltage is minimized is the anti-resonance frequency (f_a).

The constant current circuit consists of an oscillator (osc) that generates an AC current and of an input resistant R_3 , which regulates the current passing through the piezoelectric material. If R_3 is much greater than the piezoelectric

material's impedance, the output voltage across the piezoelectric material is proportional to the piezoelectric material's impedance. The frequency with the minimal output voltage is a f_r whereas and the frequency with the maximal output voltage is a f_a .

Although the constant voltage circuit gives the output voltage opposite to the output voltage of the constant current circuit, the f_r and f_a values are the positions where the piezoelectric material's impedance are at a minimum and maximum, respectively. Therefore, the constant current circuit can be substituted for the constant voltage circuit because it measures the same values f_r and f_a .

2.2 Piezoelectric Actuator and Transducer

Piezoelectric transducers are devices which convert one form of energy to another and are used in a broad range of applications such as transformers, sensors, filters, resonators and actuators (piezomotors). Actuators can convert electrical energy to mechanical energy or convert voltage and charge to force and motion. They are suitable for the following applications (Ghouti, 2000).

1. *Actuators for robots*: The capability of producing high torque (tens of Nm) by a lightweight motor is required in this application and can be easily fulfilled by an ultrasonic motor.
2. *Actuators of devices for consumer goods*: Successful applications which make full use of the flexibility of the shape, controllability and quiet operation of the motor, already exist in the car industry, in drive mechanisms for autofocus lenses in cameras etc.
3. *Actuators for precise positioning devices*: Rapid positioning devices with accuracies of the order of nanometer are being used in the production of semiconductors. Moreover, linear and rotary ultrasonic motors and appropriate control methods are being developed for various applications in positioning devices.

4. *Actuators for miniaturized machines*: Research into the use of static electrical motors and bio-actuators as drives for micro-mechanisms is also being conducted but has yet to produce some results.
5. *Actuators for machines used in space*: With high torque at low speed, they are well-suited for operating in vacuum and in the absence of the gravity in space.
6. *Actuators for material conveyors*: Because of their quiet operation, ultrasonic motors are well-suited for the conveyance of parts.

Single Layer Actuators

Longitudinal and Transverse Actuators: When an electric field having the same polarity and orientation as the original polarization field is placed across the thickness of a single sheet of piezoceramic, the piece expands in the thickness or “longitudinal” direction (i.e. along the axis of polarization) and contracts in the transverse direction (perpendicular to the axis of polarization). This is represented in Figures 2.11 (a) and (b). When the field is reversed, the motions are reversed. Sheets and plates utilize this effect. However, the motion of a sheet in the thickness direction is extremely small (on the order of tens of nanometers). On the other hand, the transverse motion along the length is generally larger (on the order of microns to tens of microns) since the length dimension is often substantially greater than the thickness. The transverse motion of a sheet laminated to the surface of a structure can induce the structure to stretch or bend, a feature often exploited in structural control systems (Transducer elements, 2007).

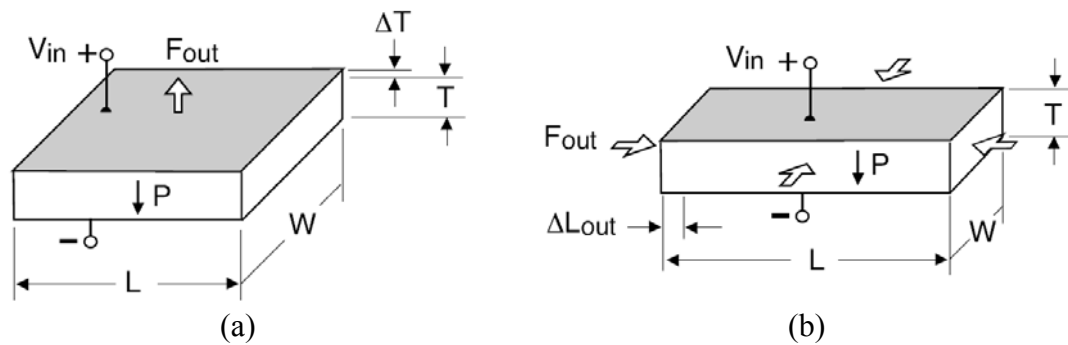


Figure 2.11 (a) Longitudinal, and (b) transverse single layer actuators (Transducer elements, 2007).

2-Layer Actuators

Two-layer elements can be made to elongate, bend, or twist depending on the polarization and wiring configuration of the layers. A center shim laminated between the two piezo layers adds mechanical strength and stiffness, but reduces motion. “2-layer” refers to the number of piezo layers. The “2-layer” element actually has 9 layers, consisting of 4 electrode layers, 2 piezoceramic layers, 2 adhesive layers, and a center shim. The two layers offer the opportunity to reduce drive voltage by half when configured for parallel operation.

Extension Actuators: A 2-layer element behaves like a single layer when both layers expand (or contract) together. If an electric field is applied which makes the element thinner, this is the cause of extension along the length and width. Typically, only motion along one axis is utilized (Figure 2.12). Extender motion on the order of microns to tens of microns, and force from tens to hundreds of Newtons is typical (Transducer elements, 2007).

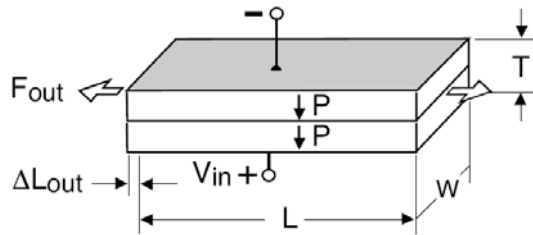
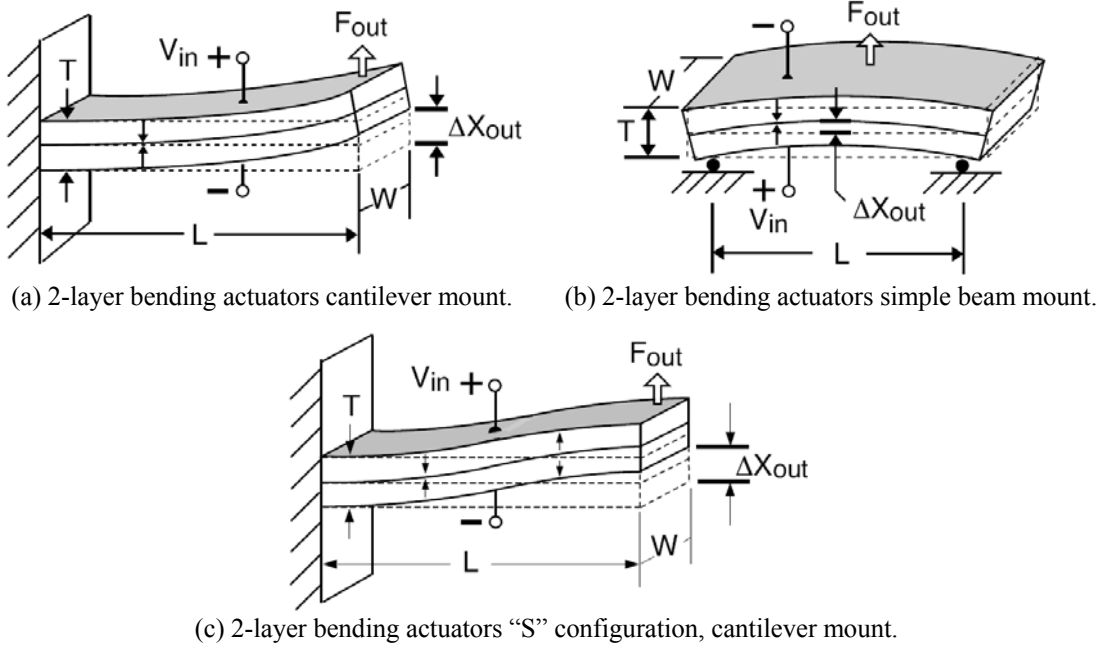


Figure 2.12 2-layer transverse actuators expanding lengthwise (Transducer elements, 2007).

Bending Actuators: A 2-layer element produces curvature when one layer expands while the other layer contracts. These transducers are often referred to as benders, bimorphs, or flexural elements. Bender motion on the order of hundreds to thousands of microns and bender force from tens to hundreds of grams is typical (Transducer elements, 2007).



Figures 2.13 Show several common bending configurations. The variety of mounting and motion options make benders a popular choice of design engineers (Transducer elements, 2007).

Multi-Layer Actuators

Any number of piezo layers may be stacked on top of one another. Increasing the volume of piezoceramic increases the energy that may be delivered to a load. As the number of layers grows, so does the difficulty of accessing and wiring all the layers. Typically, more than 4 layers become impractical.

Stack Actuators: The co-fired stack represented in Figure 2.14 is a practical way to assemble and wire a large number of piezo layers into one monolithic structure. The tiny motions of each layer contribute to the overall displacement. Stack motion on the order of microns to tens of microns, and force from hundreds to thousands of Newtons is typical (Transducer elements, 2007).

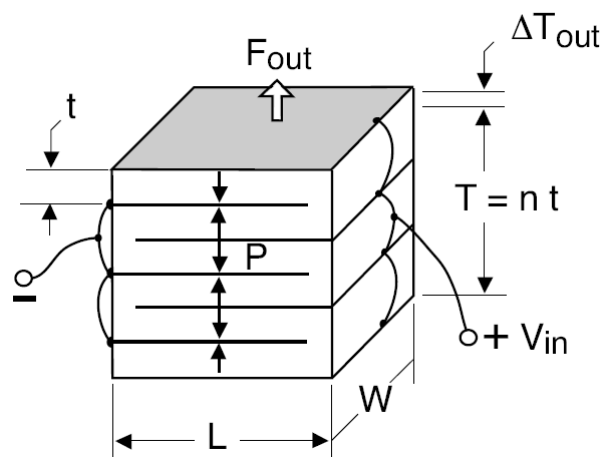


Figure 2.14 Stack actuator (Transducer elements, 2007).

A stack actuator has advantages in terms of a high generative force (100 kgf) with high efficiency (electromechanical coupling factor, $k_{33} > 70\%$), low operation voltage, response speed (10 μ s), and lifetime (10^{11} cycles) (Uchino, 1997; Newnham and Ruschau, 1991). In addition, it enables larger displacements to be generated than would be possible having a single layer in the same total thickness, for a given driving voltage (Harris *et al.*, 2006). In the stack actuator, the displacement ΔT_{out} , the capacitance C and the maximum force F_{max} produced for an actuator with n layers excited by an applied voltage V are given by:

$$\Delta T_{out} = n\Delta T = nd_{33}V \quad (2.28)$$

$$C = n \frac{\epsilon_0 \epsilon_{33} A}{t} \quad (2.29)$$

$$F_{max} = k_T \Delta T \quad (2.30)$$

where t , Δt , d_{33} , A , and k_T are the single layer thickness, displacement of a single layer, piezoelectric strain coefficient, electrode surface area and the actuator stiffness, respectively (Wang, 2002).

Actuators Performance

Piezoelectric actuators are usually specified in terms of their free deflection and blocked force. Free deflection (X_f) refers to displacement attained at the maximum recommended voltage level when the actuator is completely free to move and is not asked to exert any force. Blocked force (F_b) refers to the force exerted at the maximum recommended voltage level when the actuator is totally blocked and not allowed to move. Deflection is at a maximum when the force is zero, and force is at a maximum when the deflection is zero. All other values of simultaneous displacement and force are determined by a line drawn between these points on a force versus deflection line, as shown in Figure 2.15. Generally, a piezo motor must move for a specified amount and exert a specified force, which determines its operating point on the force against the deflection line. An actuator is considered optimized for a particular application if it delivers the required force at one half its free deflections. All other actuators satisfying the design criteria will be larger, heavier, and consume more power.

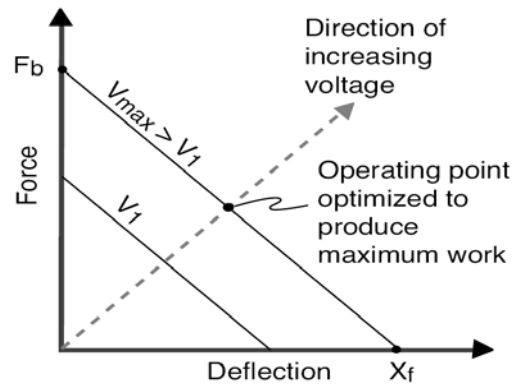


Figure 2.15 Force vs. displacement diagram for a piezoelectric actuator (Transducer elements, 2007).

Series and Parallel Operation

For actuators, series operation refers to the case where supply voltage is applied across all piezo layers at once. The voltage on any individual layer is the supply voltage divided by the total number of layers. A 2-layer device wired for series operation uses only two wires (Figure 2.16(a)), one attached to each outside electrode. Parallel operation refers to the case where the supply voltage is applied to each piezo layer individually. This means accessing and attaching wires to each layer. A 2-layer bending motor wired for parallel operation requires 3 wires (Figure 2.18(b)), one attached to each outside electrode and one attached to the center shim. For the same motion, a 2-layer motor poled for parallel operation needs only half the voltage required for series operation and has four times the capacitance.

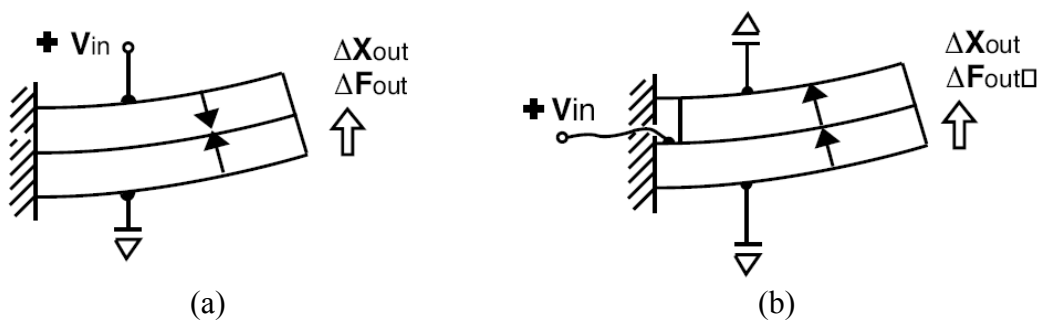


Figure 2.16 A 2-layer bending actuators; Poled for Series (2-wire) and Parallel Operation (3-wire) (Transducer element , 2007).

2.3 Composite Materials

Many of our modern technologies require materials with unusual combinations of properties that cannot be met by the conventional metal alloys, ceramics, and polymeric materials. In the present, composite or multiphase materials are popular and developed continually because of their various properties. Many composite materials are composed of just 2 phases; one is termed the matrix which is continuous and surrounds the other phase often called the dispersed phase. The properties of composites are a function of the properties of constituent phases, their relative amounts, and geometry of dispersed phase. “*Dispersed phase geometry*” in this context means the shape of the particle size, distribution, and orientation (William and Callister, 2005).

The 0-3 composite connectivity

The most commonly studied composites are 0-3 and 1-3 configurations and the former one owed popularity to the easy and convenient fabrication procedure which allows for commercial production at a relatively low cost (Dias and Das-Gupta, 1996). The 0-3 composites may be produced by mixing the ceramic particles in a hot rolling mill with softened thermoplastic polymer, and forming process can be made at room temperature. The following equation can be used to prepare the quantities required for mixing of the ceramic and polymers (Lang and Das-Gupta, 2000).

$$M^c = M^p \times \frac{\rho^c}{\rho^p} \times \frac{\phi}{1-\phi} \quad (2.31)$$

where M , ρ and ϕ are the mass, density, and volume fractions respectively, and the subscripts P and C refer to the polymer and ceramic respectively. The density ρ of the composite is determined thus

$$\rho = \phi\rho^c + (1-\phi)\rho^p \quad (2.32)$$

and the total composite volume V is given by

$$V = \frac{M^c}{\phi \rho^c} \quad (2.33)$$

2.4 Tape Casting Technique

There are many techniques for forming material. The one is “*tape casting*” which is applied to this work. As the name implies, thin sheet of flexible tape are produced by means of a casting process. These sheets are prepared from slips, in many respects similar to those employed for slip casting. This type of slip consists of a suspension of ceramic particles in an organic liquid that also contains binder and plasticizers that are incorporated to impart strength and flexibility to the cast tape. The actual tape is formed by pouring the slip onto a flat surface (of stainless steel, glass, a polymeric film, or paper). A doctor blade spreads the slip into a thin tape of uniform thickness, as shown schematically in Figure 2.17. After thin tape has been formed, retains significant porosity, low density, and insufficient strength for practical application. Moreover, it may still contain some liquid (e.g., water or solvent), which was added to assist in the forming operation. These things are improved or removed in drying and annealing process. During annealing operation, the density is further increased (with an attendant decrease in porosity) and the mechanical strength is enhanced. The one thing is taken into consideration. During the tape is cooled from elevated temperature. The internal stress or thermal stress may be introduced as a results of the difference in cooling rate and thermal contraction between the surface and interior regions. These thermal stresses are important in brittle ceramics or non-uniform properties in composites. Normally, attempts are made to avoid thermal stresses, which may be accomplished by cooling the piece at a sufficiently slow rate. Tape thickness is normally between 0.1 to 2 mm (0.004 to 0.08 in.) (William and Callister, 2005).

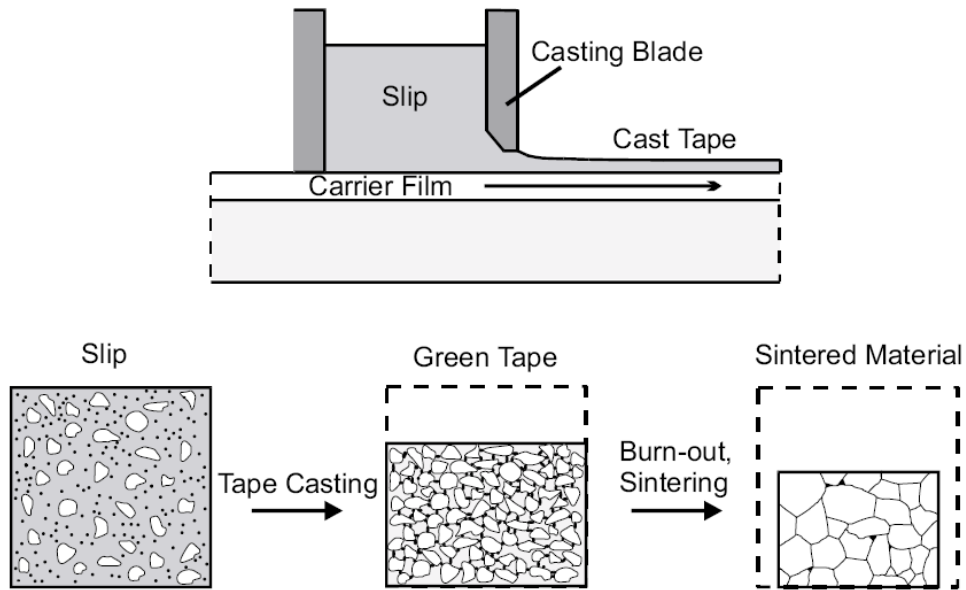


Figure 2.17 Schematic diagram showing the tape casting process (Mistler *et al.*, 1978).

2.5 Overall Properties of BaTiO₃ and PVDF

The samples used in the present work were the 0-3 connectivity composites, which consisted of ceramic BT and polymer PVDF as described below.

The barium titanate or BaTiO₃ ceramic is one of the most intensively studied ferroelectric materials and used in various applications such as electromechanical applications, electro-optic, electronic component. BaTiO₃ has an A^{II}B^{IV}O₃ type perovskite structure. A general unit cell of a cubic perovskite was shown in Figure 2.18. Below the Curie point (~130 °C), the structure is slightly distorted to the tetragonal form with a dipole moment along the c direction. Other transformations occur at temperature close to 0 °C and -90 °C. Below 0 °C, the unit cell is orthorhombic with the polar axis parallel to a face diagonal and it is rhombohedral with the polar axis along a body diagonal below -90 °C. The transformations are illustrated in Figure 2.19.

A consideration of the ion displacements accompanying the cubic-tetragonal transformation can give insight into how the spontaneous polarization might be coupled from unit cell to unit cell. X-ray studies have established that in the tetragonal form, taking the 4 central (B) oxygen ions in the cubic phase as origin, the

other ions are slightly shifted as shown in Figure 2.20. It is evident that if the central Ti^{4+} ion is closer to one of the O^{2-} ions marked A, it will be energetically favorable for the Ti^{4+} ion on the opposite site of the A to be located more distantly from that O^{2-} ions, thus engendering a similar displacement of all the Ti^{4+} ions are displaced in the same direction.

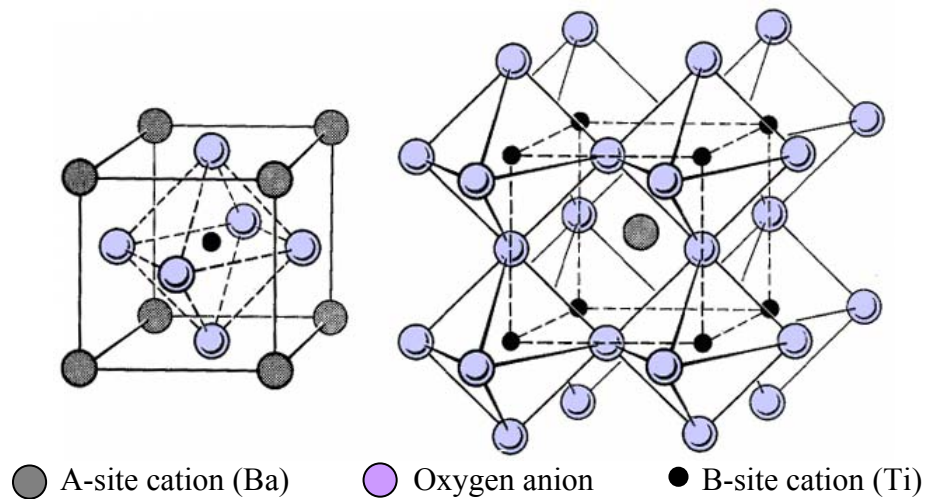


Figure 2.18 A cubic perovskite unit cell showing the oxygen octahedral and the ionic positions for the A and B cations.

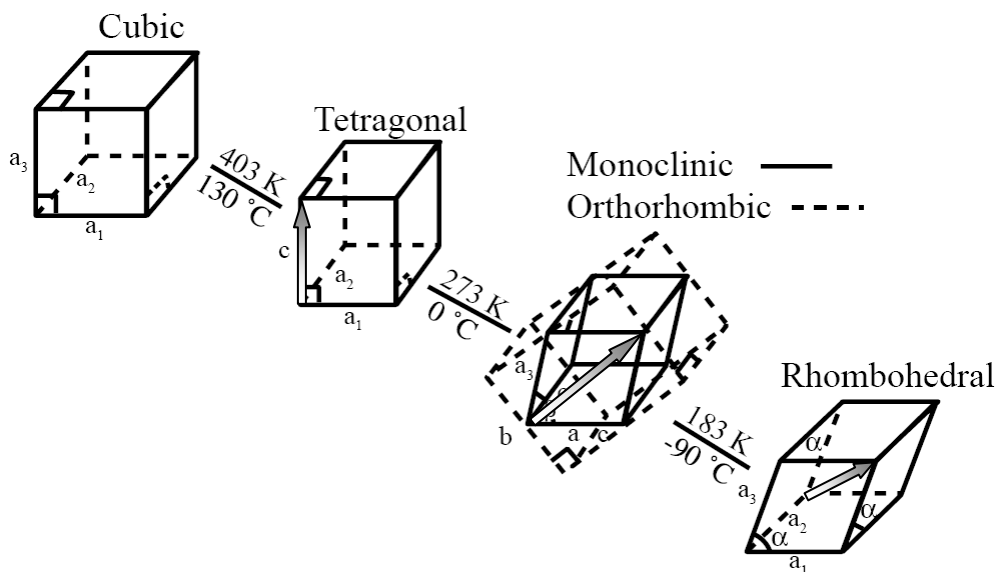


Figure 2.19 Unit cell distortions of BT single crystals ; \rightleftharpoons represents direction of dipole moment (Kay and Vousdan, 1949; Moulson and Herbert, 1990).

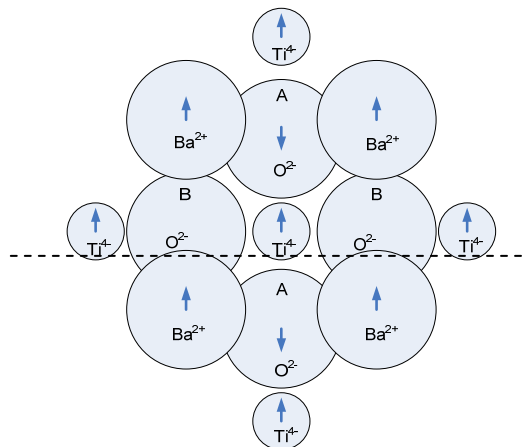


Figure 2.20 Approximate ion displacements in the cubic-tetragonal distortion in BT (Moulson and Herbert, 1990).

Interest in the electrical properties of PVDF has began since 1969 when Kawai (Kawai, 1969) showed that poled thin films that had been poled exhibited a very large piezoelectric coefficient, 6-7 pC/N, and a value which is about 10 times larger than those observed in any other polymer. PVDF molecules have a repeat unit of $-\text{CH}_2\text{-CF}_2-$ and are typically 50 to 60% crystalline depending on thermal and processing history. The morphology of PVDF consists of crystallites dispersed within amorphous regions. The degree of crystallinity present in such polymers depends on their method of preparation and thermal history. Most semicrystalline PVDF has at least 4 polymorphic phases (Figure 2.21), i.e., α -, β -, γ -, δ -phases. The nonpolar α -phase is the most common structure of PVDF, and the other 3 phases are polar.

Mechanical orientation, thermal annealing and high voltage treatment have all been shown to be effective in inducing crystalline phase transformations. Stretching the polymer essentially aligns the amorphous strands in the film plane as shown in Figure 2.22 and facilitates uniform rotation of the crystallites by an electric field. Electrical poling is accomplished by applying an electric field across the thickness of the polymer. An electric field on the order of 50 MV/m is typically sufficient to effect crystalline orientation. Polymer poling can be accomplished using a direct contact method or a corona discharge. The latter method is advantageous

since contacting electrodes are not required and large area samples can be poled in a continuous fashion.

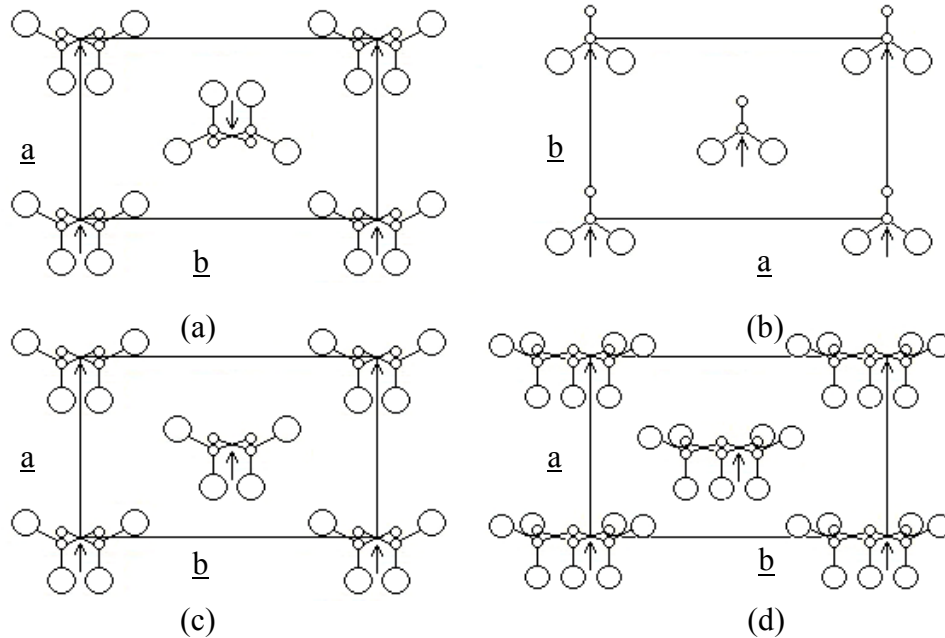


Figure 2.21 Unit cells of PVDF phases when project on a plan that perpendicular to the c axis; (a) α -phase, (b) β -phase, (c) γ -phase, and (d) δ -phase. When (o) and (O) represent carbon and fluorine atom, respectively (not show hydrogen atom) (Lovinger, 1983).

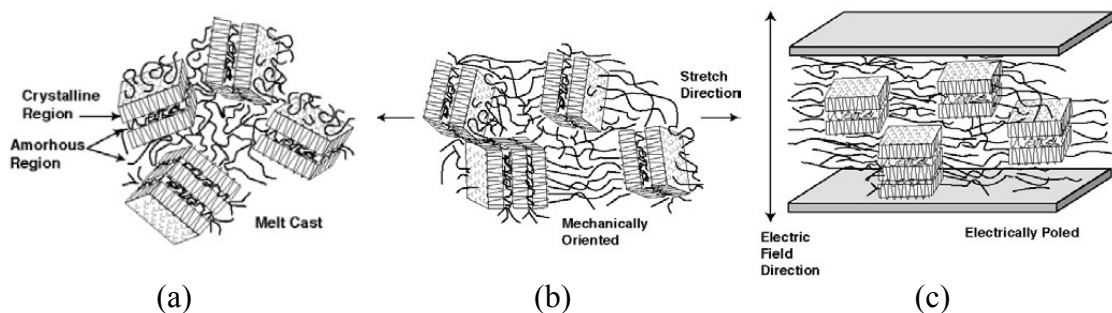


Figure 2.22 (a) Schematic illustration showing random stacks of amorphous and crystal lamellae in PVDF polymer, (b) crystalline phase transformation due to mechanically stretching and (c) crystalline orientation in PVDF under the applied high electric field (Harrison and Ounaies, 2001).

The β -phase of PVDF is probably the most important of the 4 polymorphs in piezoelectric and pyroelectric applications. The β -phase has orthorhombic structure with $mm2$ symmetry. The dipole moment of the polymer chain in the β -phase is 7.0×10^{-30} C·m, and it lies normal to the chain direction. Each crystallite of the β -phase has a dipole moment. The random orientation of crystallites has not net polarization until it is poled by an application of an external electric field, which encourages a dipolar orientation of the crystallites. The piezo- and pyroelectricity of PVDF are directly associated to the field induced polarization of the β -phase crystallites. This polarization arises from the alignment of the C-F dipoles of the β -phase polymer chains in the electric field direction (Figure 2.23).

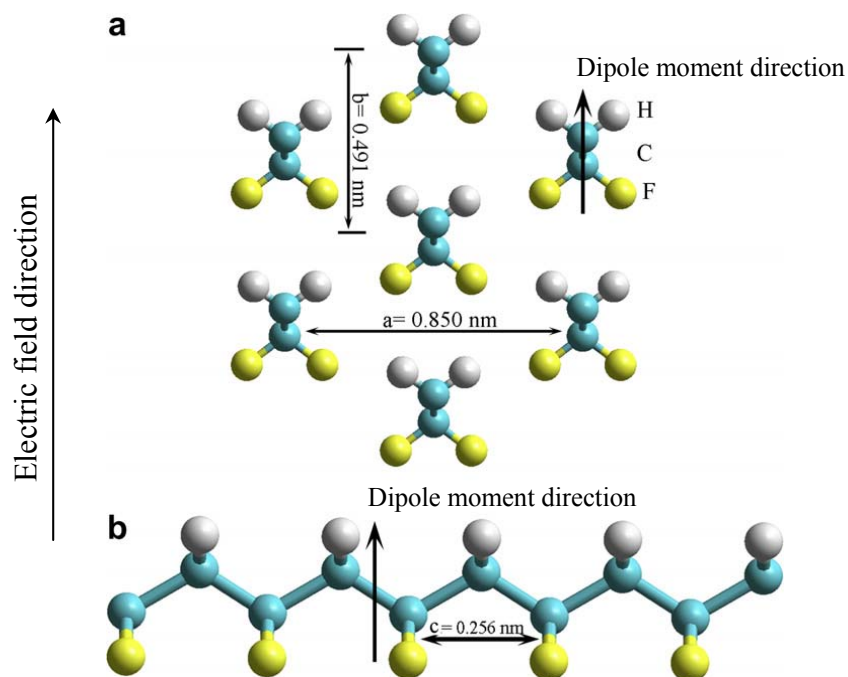


Figure 2.23 Structure of β -phase PVDF (Zhu *et al.*, 2008).

CHAPTER 3

EXPERIMENTALS

This chapter presents the details of the experimental procedure involving the preparation and characterizations of the BT-PVDF composites. The characterizations include the physical and dielectric properties followed by the determination of most relevant electromechanical coupling using the resonance method. Thereafter, the piezoelectric stacks are made from the composite samples and determined the electromechanical coupling. The experimental results of the stacks are then compared with those from the finite element analysis.

3.1 Materials

- 3.1.1 Commercial polyvinylidene fluoride (PVDF) powder (Aldrich)
- 3.1.2 1-Methyl-2-pyrrolidone (NMP) solution (Fluka 69120, 98 % purity)
- 3.1.3 Barium titanate powder (Aldrich, 99 % purity) with average particle size of 3 μm
- 3.1.4 Acetone
- 3.1.5 Thermally conductive adhesive (RS 850 984)
- 3.1.6 SPI conductive silver paint (SPI Supplies[®])
- 3.1.7 Copper wire
- 3.1.8 Glass plate

3.2 Apparatus

- 3.2.1 High voltage power supply (Stanford Research Systems model PS 350/5000V–25W)
- 3.2.2 pA meter/DC voltage source (Hewlett Packard model 6451B)
- 3.2.3 Corona poling setup

- 3.2.4 Thermometer (Hanna instrument model HI 8757)
- 3.2.5 Soldering iron (Hisatomi model OP 60L)
- 3.2.6 Hot plate (PNP model HS-2)
- 3.2.7 Magnetic stirrer
- 3.2.8 Hot plate (Chemat model KW-4AH)
- 3.2.9 Beaker (volume 100 ml)
- 3.2.10 Digital electronic balance (Cahn model 7550)
- 3.2.11 Multimeter (Fluke model 8840A)
- 3.2.12 Multimeter (Digicon model BM-870A)
- 3.2.13 Plastic spatula
- 3.2.14 forceps
- 3.2.15 LCR meter (Hewlett Packard model HP 4263B) with dielectric test fixture model HP 16451B
- 3.2.16 Oscilloscope (Tektronix model TDS 420A)
- 3.2.17 30 MHz Synthesized Function Generator Model DS 345
- 3.2.18 Constant voltage circuit setup
- 3.2.19 Electrometer (Keithley Model 6514)
- 3.2.20 Lock-in amplifier (Standford Reseach Systems model SR 530)
- 3.2.21 Thickness Gauge Handing (Peacock Model G-7C, resolution 0.001 mm)
- 3.2.22 Vernier calipper

3.3 Experimental Procedure

3.3.1 BaTiO₃-PVDF Composite Preparation

In the preparation process, the quantity of 0.15 volume fraction of the BT powders was calculated from Equation (2.31). The low volume fraction of the ceramic was used in order to assure that the ceramic particles were dispersed uniformly in the polymer matrix without interconnection among the powders (Hajeesaeh and Muensit, 2006).

For the polymer matrix, the 1-methyl-2-pyrrolidone (NMP) solvent of 10 %wt and the PVDF powder of 90 %wt were under mixing before being boiled at 200 °C. The PVDF solution was then stirred at 60 °C for 2 h. And used as the matrix of the BT particles. The BT-PVDF mixture was then stirred at 60 °C for 4 h (Figure 3.1). Figure 3.2 shows the heat treatment conditions used in the composite sample preparation.



Figure 3.1 Illustration of the apparatus necessary for the sample preparation.

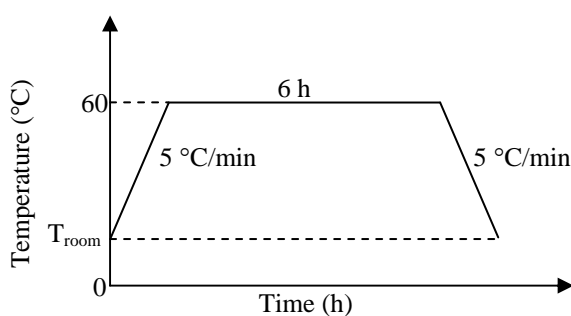


Figure 3.2 Heat treatment conditions used in the composite sample preparation.

The tape casting technique was used to shape the treated mixture. A glass plate (Figure 3.3) with clean surfaces was used as a base or substrate. The viscous solution was poured onto the glass plate, and the thickness of each casted sample was controlled by fixing the height of a blade at a constant height which was later moved across the poured solution.

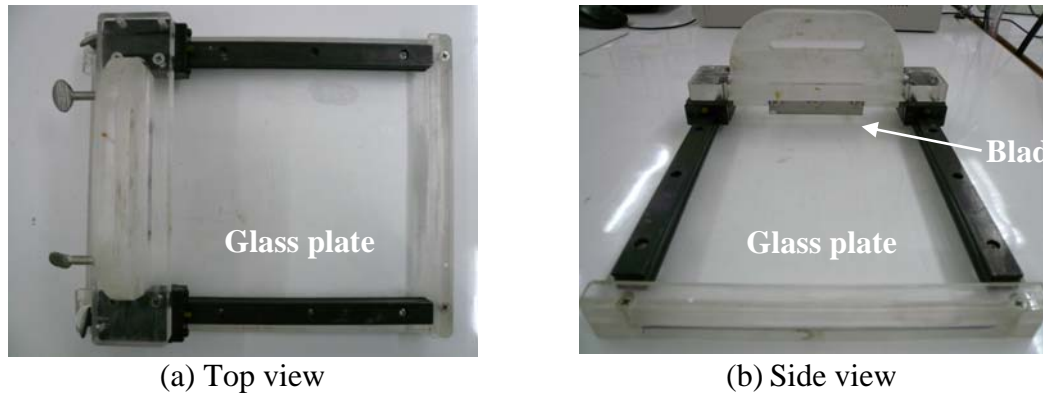


Figure 3.3 A glass plate of an area of $15 \times 15 \text{ cm}^2$ with a blade for tape casting.

After the tape was formed, it still remained porous with insufficient strength. An annealing process was applied to the taped sample at $120 \text{ }^\circ\text{C}$ for 6 h (Figure 3.4). The NMP solvent was all evaporated and the density of the dried sample was determined.

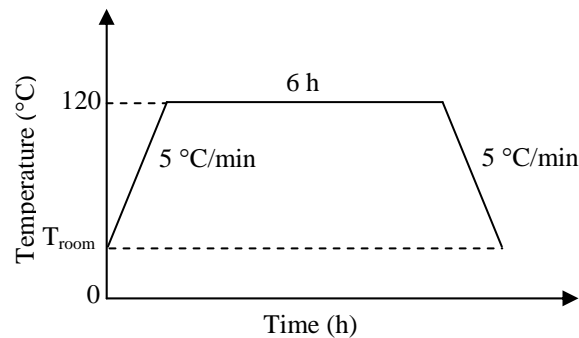


Figure 3.4 Heat treatment conditions for an annealing process.

Finally, the tape-casted BT-PVDF was cut into pieces of dimension of about $10 \times 10 \text{ mm}^2$. These samples were divided into 3 groups:

- 1) Unpoled sample.
- 2) Polymer-poled sample, the corona poling method was used to pole the PVDF phase with a DC electric field of 500 MV/m for 20 min

(Dasaesamoh, 2008). Illustrations of the poling process were in Figures 3.5 and 3.6

3) Sample with both phases active, the sample with poled PVDF phase was subsequently poled the BT phase in opposite direction under the applied field -25 MV/m at room temperature for 15 min (Limbong and Guy, 1998). This condition was chosen in order to enhance the piezoelectric activity of composite (Bloss *et al.*, 2001)

In conclusion, the sample preparation procedure was schematically shown in Figure 3.7.

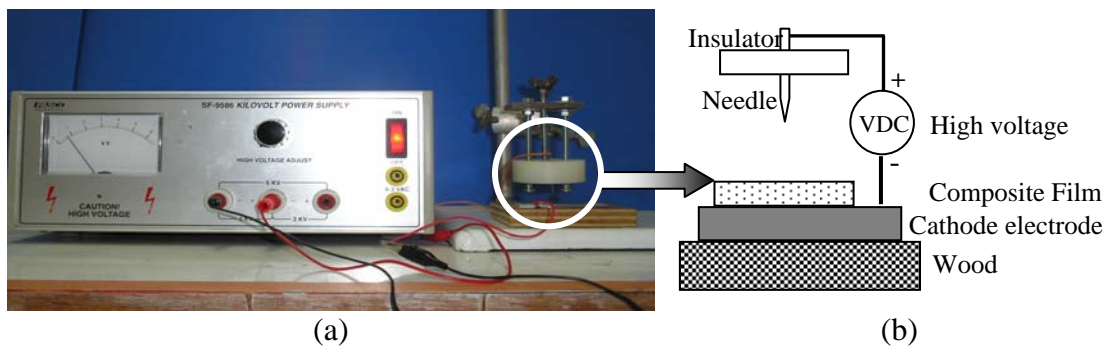


Figure 3.5 A corona poling setup. (a) The apparatus for the corona poling and (b) the details of the connected parts in (a).

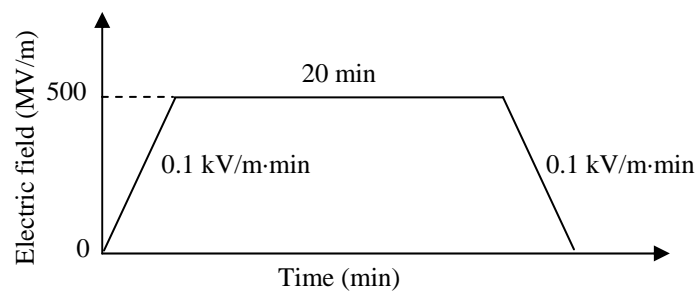


Figure 3.6 The application of a DC electric field during the poling of the PVDF (Dasaesamoh, 2008).

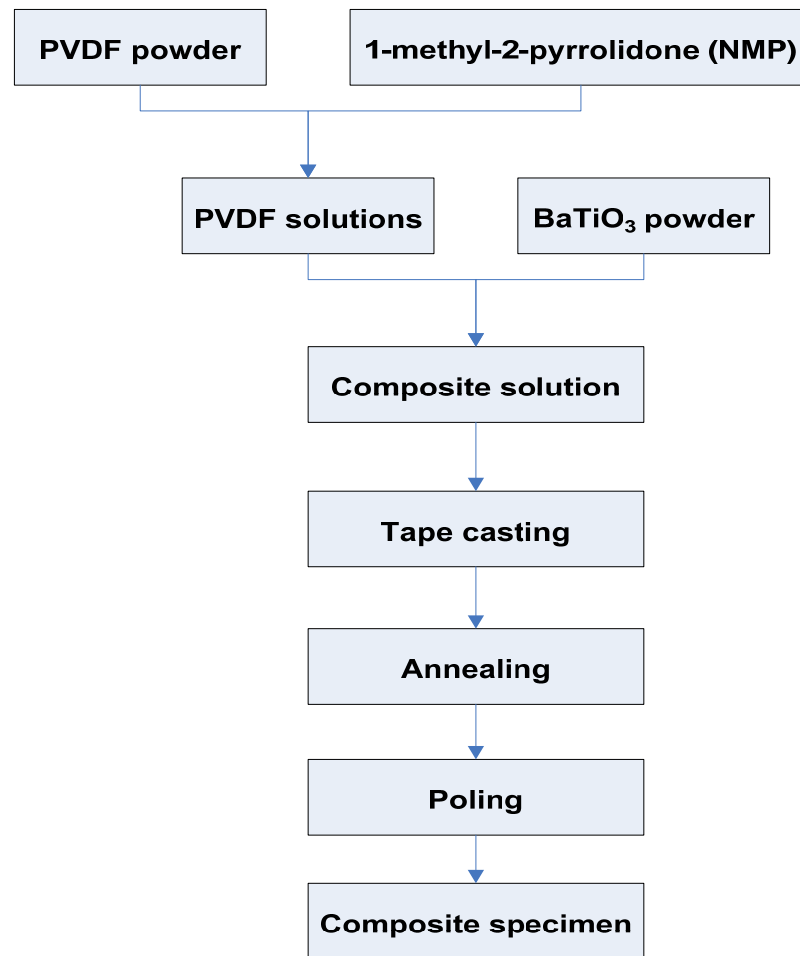


Figure 3.7 A schematic diagram of the preparation of the BT-PVDF composites.

3.3.2 Physical Characterization

The density of the sample was determined using Equation (2.32). By using the thickness gauge (Figure 3.8), the thickness can be averaged for the composite from a measurement at 3-5 different points on the same sample.



Figure 3.8 Thickness gauge handing.

3.3.3 Electrical Characterization

Each sample was electroded by a silver paint and heated at 60 °C for 20 min. The capacitance of the sample was measured at room temperature by the LCR meter at 0.1, 0.12, 1, 10 and 100 kHz (Figure 3.9). The results were used to calculate the dielectric constant. The dielectric loss for all samples was directly observed from the LCR meter.

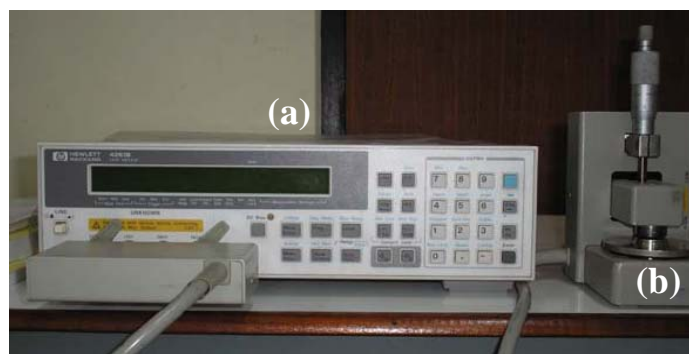


Figure 3.9 (a) HP 4263B LCR meter and (b) a test fixture 16451B.

The following operations were performed after switching on the LCR meter in order to reduce residual impedance and stray admittance in the test fixture.

OPEN Correction

The stray admittance in the test fixture can be reduced by performing the following procedure.

- a) Turn the small knob of the test fixture counterclockwise (ccw) to move the Guarded/Guard electrode away from the Unguarded electrode.
- b) Connect the attachment with the cover to the Guarded/Guard electrode after removing the covers of both electrodes shown in Figure 3.10.

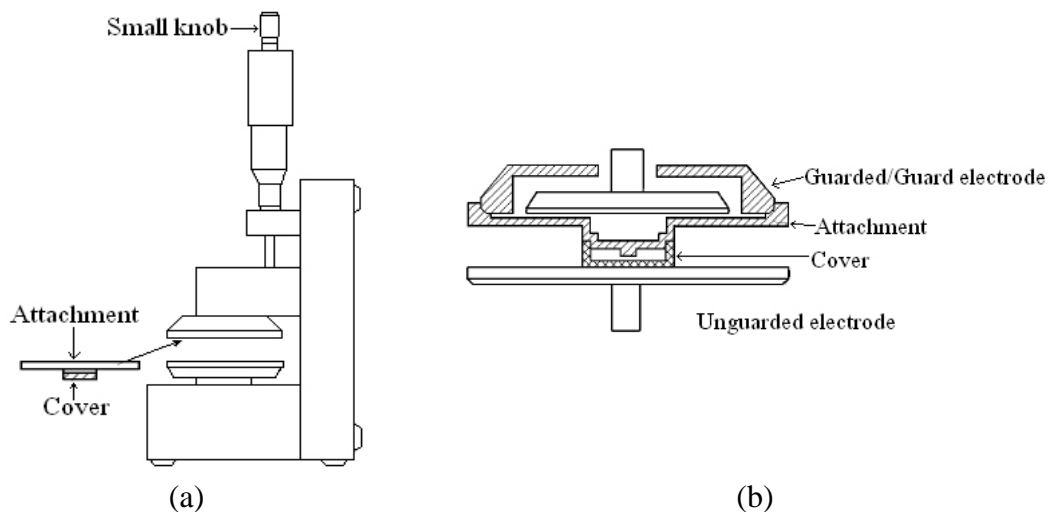


Figure 3.10 (a) The attachment connected to the Guarded/Guard electrode for OPEN correction; (b) the details of the connected parts in (a).

- c) Turn the small knob of the test fixture clockwise (cw) to bring the Unguarded electrode into contact with the attachment (until the clutch slips). As shown in Figure 3.10 (b), the inner electrode of the Guarded/Guard electrode is completely surrounded by the guard.
- d) Perform the OPEN correction measurement by pressing Blue - Open. The OPEN correction menu is displayed (Figure 3.11).

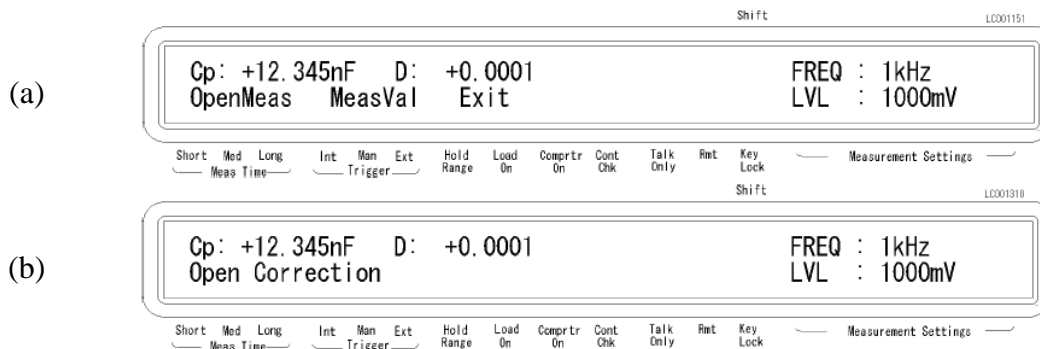


Figure 3.11 Illustration of the messages appeared on the LCR meter display; (a) during the OPEN correction performance; (b) when the OPEN correction is complete.

- e) Press Arrow key until Openmeas blinks, and press Enter. The OPEN correction is performed. During that time, the following message is displayed. After a while, the LCR meter completes OPEN correction with the message Open Correction Complete
- f) Turn the small knob ccw to move the electrodes away from each other, and remove the attachment.

SHORT Correction

The procedure to perform SHORT correction depends on the type of the Guarded/Guard electrode used. Therefore, it should select the appropriate procedure according to the used Guarded/Guard electrode. In this work, the Guarded/Guard electrode type-B (diameter 5 mm) and type-D were chosen. The residual impedance in the test fixture can be reduced by performing the following SHORT correction procedure.

- a) Turn the small knob ccw to move the Guarded/Guard electrode away from the Unguarded electrode then remove the cover from both electrodes.
- b) Remove the cover from the attachment when the Guarded/Guard electrode type-B is used. Then connect the attachment to the

Unguarded electrode as shown in Figure 3.12 (a) and 3.12 (b), respectively.

- c) Turn the small knob cw to contact the Guarded electrode to the Unguarded electrode for the Guarded/Guard electrode type-D as shown in Figure 3.12 (c). The knob cannot be turned around until the Guard electrode is contacted with the Unguarded electrode.

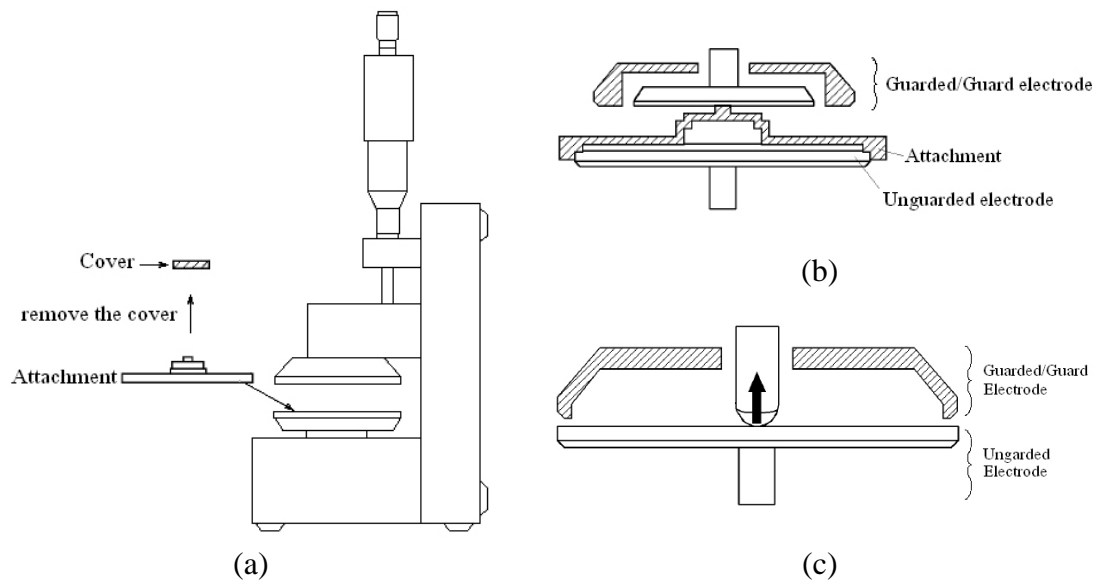


Figure 3.12 (a) Connecting the attachment to the Unguarded electrode; (b) the details of the connected parts in (a).

- d) Perform the SHORT correction measurement by pressing Blue – Short. The SHORT correction menu is displayed (Figure 3.12 (a)).
- e) Press the Arrow key until Shortmeas blinks, and press Enter. The SHORT correction is performed. During that time, the following message is displayed. After a while, the LCR meter completes SHORT correction with the message “SHORT Correction Complete” (Figure 3.13 (b)).
- f) Turn the small knob ccw to move the electrodes away from each other and remove the attachment for the electrode type-B.

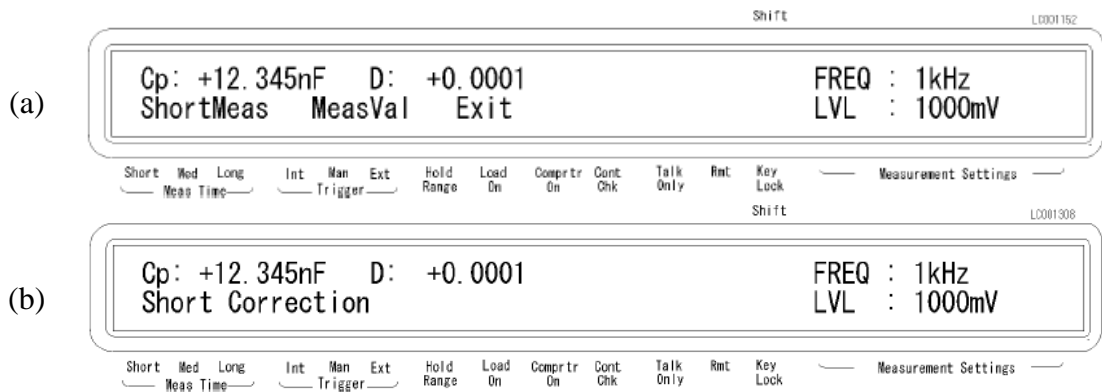


Figure 3.13 Illustration of the messages appeared on the LCR meter display; (a) during the SHORT correction performance; (b) when the SHORT correction is complete.

Measurement Method

1. Place a sample between the Guarded/Guard electrode and Unguarded electrode.
2. Turn the small knob ccw to contact the Guarded/Guard electrode to the composite.
3. Set the applied voltage at 1 V and choose measurement mode as capacitance (C_p) and dissipation factor (D).
4. Record the C_p and D at 100 Hz, 1 kHz, 10 kHz and 100 kHz.
5. Calculate the dielectric constant.
6. Plot a graph of the dielectric constant as a function of frequency.

3.3.4 Electromechanical Characterization

The sample with both surfaces painted with the conducting glue was under the resonance measurement using the constant voltage circuit (Figure 3.14 or Figure 2.9). This experimental setup was shown in Figure 3.15 and the measurement procedure is as follows.

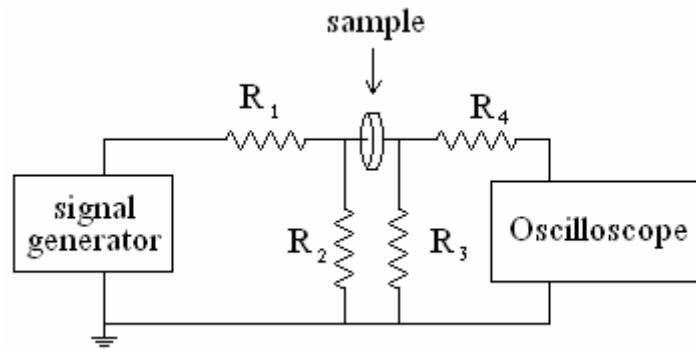


Figure 3.14 A schematic diagram of a constant voltage circuit.

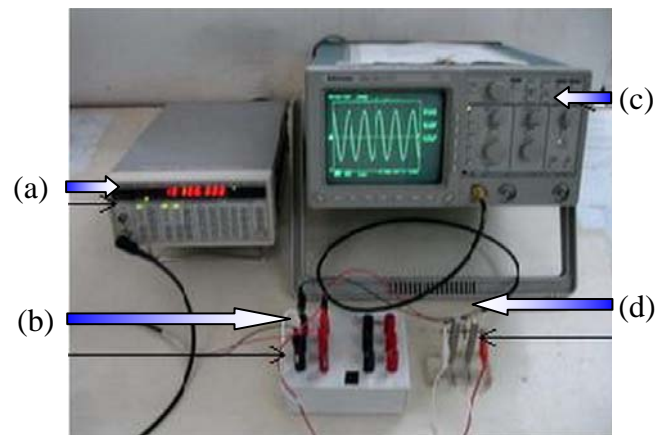


Figure 3.15 Experimental setup for the resonance measurement : (a) Function generator, (b) constant voltage circuit, (c) oscilloscope and (d) sample clamer.

- 1) Clamp a sample with a sample clamer/holder.
- 2) Turn on the function generator and the oscilloscope (warm up times ≥ 30 minutes).
- 3) Apply a start frequency of a sinusoidal signal from the function generator to the constant voltage circuit. A signal amplitude was kept constant at 5 V.
- 4) Monitor the output voltage by the oscilloscope.
- 5) Repeat the measurement procedure with increasing frequency to the maximum frequency of the LCR meter.
- 6) Plot a graph between the output voltage and frequency.

- 7) Determine the resonance and antiresonance frequencies, including calculate the k_{31} value using a formula for a rectangular plate.

3.3.5 Fabrication of Piezoelectric Stack

From Figure 3.16, each side of the samples was glued together with the silver paint in order to make a stack. Each stack contained the samples of the same group (the unpoled samples were not stacked). The number of the layers in the stacks, n was varied to be 1, 2, 3 and 4. The silver paint was also used as the internal electrodes inside the stack.

3.4 Finite Element Analysis

The resonance and antiresonance frequencies of BT-PVDF multilayered stack were analyzed by means of the FEA and the software MSC.MARC 2005r2. The conditions of the model used in the FEA are:

- The stack consists of the alternating layers of the sample and the silver paint
- The thickness of the sample and the silver paint are equal.
- The BaTiO₃-PVDF composite layers are composed of the BaTiO₃ particles and the PVDF polymer.
- The volume ratio of BaTiO₃ to PVDF is 15 : 85.
- The BaTiO₃ particles are randomly embedded in PVDF polymer matrix.
- The silver paint layers are used as conductive and adhesive layers.
- Each BaTiO₃, PVDF and silver paint layers have similar properties.
- To simplify the analysis, the 2-D model of stack is used and the effect of electric wire is neglected.

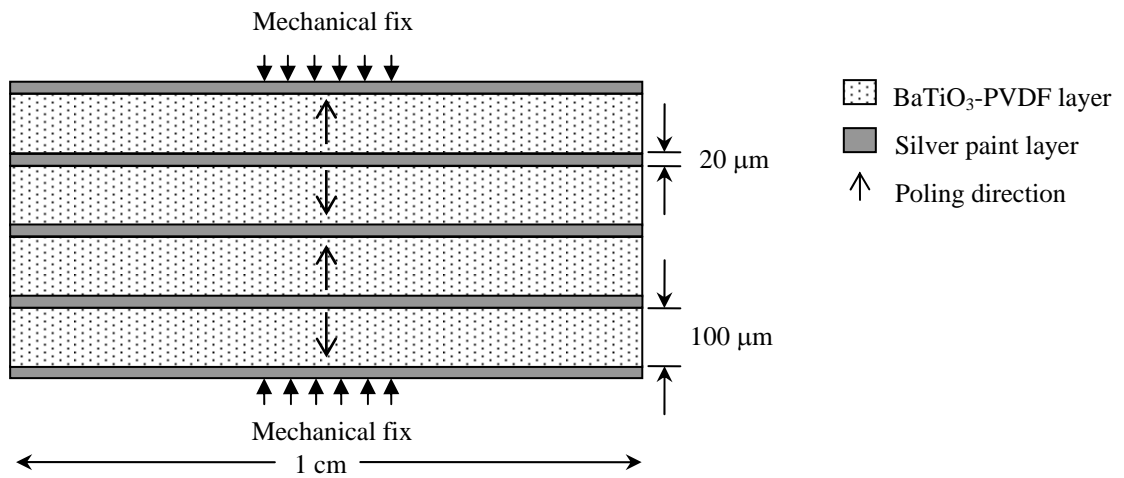


Figure 3.16 The sketch of the 2-D stack.

The element type used for the meshing of the FEA model was the element type 11 (i.e., a quadrilateral plane-strain). For the silver paint, BT and PVDF layers used were the element type 161 (i.e., a plane-strain piezoelectric quadrilateral). A stacked transducer model in MSC.MARC[®] 2005r2 requires the permittivity, the piezoelectric and the elastic coefficient matrices specified. These matrices were listed in Table 3.1.

Table 3.1 Material properties used in the FEA.

Materials	Properties	Matrices
BaTiO ₃	Density (kg/m ³) (Sakakibara <i>et al.</i> , 1994)	5,800
	Elastic stiffness (N/m ²) (Li <i>et al.</i> , 1996)	$10^9 \times \begin{bmatrix} 211 & 107 & 114 & 0 & 0 & 0 \\ 107 & 211 & 114 & 0 & 0 & 0 \\ 114 & 114 & 160 & 0 & 0 & 0 \\ 0 & 0 & 0 & 56.2 & 0 & 0 \\ 0 & 0 & 0 & 0 & 56.2 & 0 \\ 0 & 0 & 0 & 0 & 0 & 127 \end{bmatrix}$

Table 3.1 Material properties used in the FEA (continued).

Materials	Properties	Matrices
BaTiO ₃	Piezoelectric coefficient (m/V) (Li <i>et al.</i> , 1996)	$10^{-12} \times \begin{bmatrix} 0 & 0 & 0 & 0 & 580 & 0 \\ 0 & 0 & 0 & 580 & 0 & 0 \\ -50 & -50 & 106 & 0 & 0 & 0 \end{bmatrix}$
	Permittivity (F/m) (Li <i>et al.</i> , 1996)	$10^{-7} \times \begin{bmatrix} 0.3630 & 0 & 0 \\ 0 & 0.3630 & 0 \\ 0 & 0 & 0.0112 \end{bmatrix}$
PVDF	Density (kg/m ³) (Sakakibara <i>et al.</i> , 1994)	1,780
	Elastic stiffness (N/m ²) (Varadan <i>et al.</i> , 1989)	$10^9 \times \begin{bmatrix} 3.61 & 1.61 & 1.42 & 0 & 0 & 0 \\ 1.61 & 3.13 & 1.31 & 0 & 0 & 0 \\ 1.42 & 1.31 & 1.63 & 0 & 0 & 0 \\ 0 & 0 & 0 & 0.55 & 0 & 0 \\ 0 & 0 & 0 & 0 & 0.59 & 0 \\ 0 & 0 & 0 & 0 & 0 & 0.69 \end{bmatrix}$
	Piezoelectric coefficient (m/V) (Varadan <i>et al.</i> , 1989)	$10^{-12} \times \begin{bmatrix} 0 & 0 & 0 & 0 & -19.55 & 0 \\ 0 & 0 & 0 & -20.56 & 0 & 0 \\ 14.13 & 2.02 & -28.26 & 0 & 0 & 0 \end{bmatrix}$
	Permittivity (F/m)	$10^{-10} \times \begin{bmatrix} 0.6109 & 0 & 0 \\ 0 & 0.7614 & 0 \\ 0 & 0 & 0.6729 \end{bmatrix}$
Silver paint	Density (kg/m ³) (SPI supplies [®] , 2008)	1,710
	Young's modulus (N/m ²) (SPI supplies [®] , 2008)	4×10^{10}
	Poisson ratio (SPI supplies [®] , 2008)	0.35

CHAPTER 4

RESULTS AND DISCUSSIONS

4.1 Physical Properties

The density of the BT-PVDF composites prepared in this work was $2,425 \text{ kg/m}^3$ and the average thickness was $100 \pm 0.5 \text{ }\mu\text{m}$. Figure 4.1 shows a picture of the composites.



Figure 4.1 Pictorial view of a composite tape (upper) which was cut into pieces with dimensions of about $10 \times 10 \text{ mm}^2$ (lower).

4.2 Dielectric Properties

Figure 4.2 shows the plot of calculated ϵ_r' as a function of frequency. The measured dielectric loss was also plotted against the frequency in the same figure.

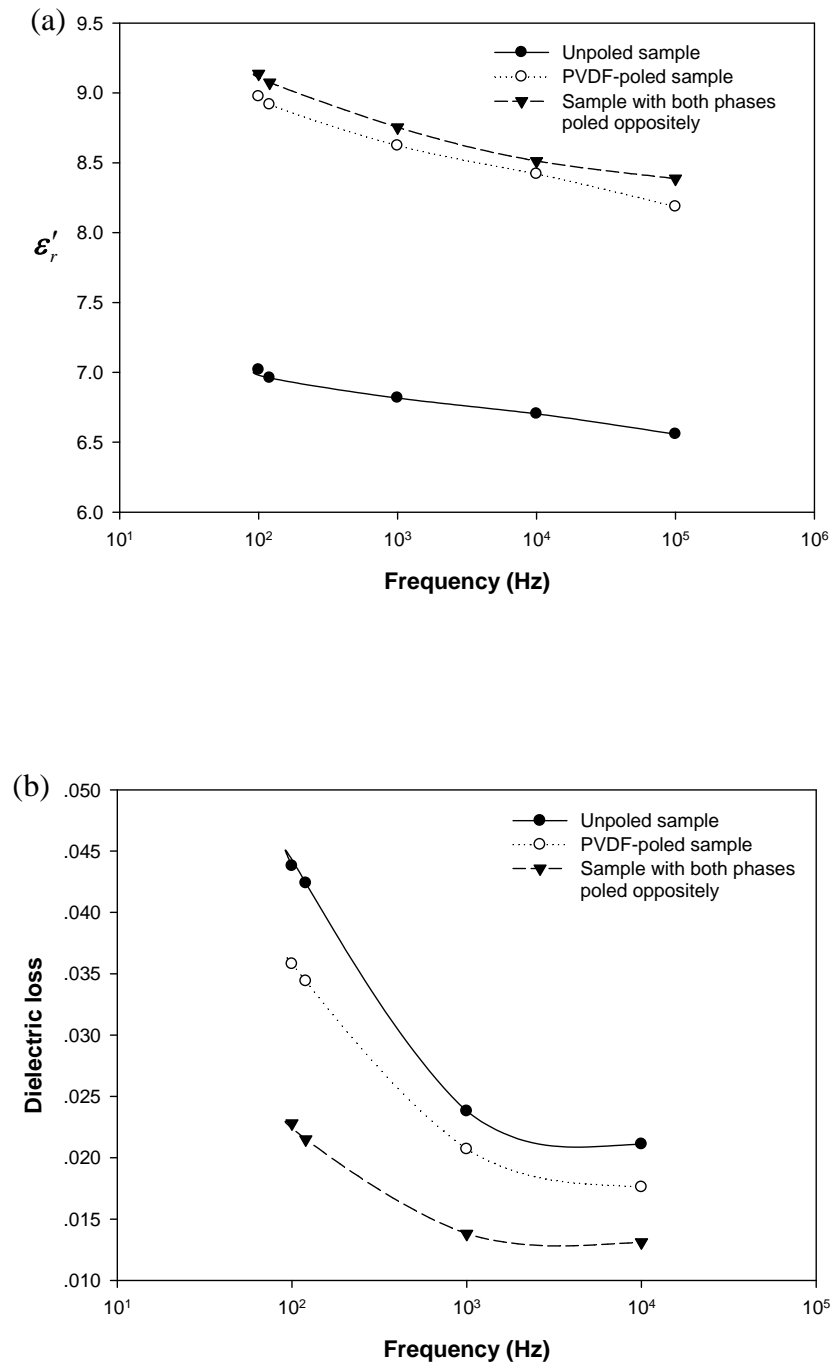


Figure 4.2 The experimental data of the (a) dielectric constant, and (b) dielectric loss as a function of frequency for the BT-PVDF composites.

From Figure 4.2, the sample without poling has the lowest dielectric constant. These values for the samples with PVDF poled and with both phases poled are slightly different. This was because i) the poling electric field induced the alignment of the dipole moment and ii) the poling of the ceramic in opposite direction did not change the polarization of the polymer. This led to an increase in the net polarization of the composites. The dielectric loss of the sample with both phases poled oppositely was, in contrast, minimized. This was due to the influence of the poling field upon the elastic and porous nature of the PVDF polymer as well as the low-capacitive nature of the BT ceramic.

4.3 Electromechanical Property of the Piezoelectric Stack

The poled samples were glued together and the variations of the resonance and antiresonance for all stacking samples were shown in Figure 4.3. The output voltage was found to be proportional to the stacking samples' admittance (results were not shown here). Each stacking sample exhibited the maximum and minimum admittance at the resonance and antiresonance, respectively.

Figure 4.4 displays an increased in the resonant frequency as the number of the stack increased. A change in the antiresonance was in a similar manner. A relationship represented for the variations of the resonance and antiresonance was graphically fitted and mathematically found to be:

$$f = 107.59n + 269.54 \quad (4.1)$$

where f is the resonant frequency, n is the number of the layers and C is a constant. The slope and the intercept depend on the type of piezoelectric materials and structure of the stack. It is anticipated that the stack with layer of the two-phase poled opposite will display a relationship similar to Equation (4.1).

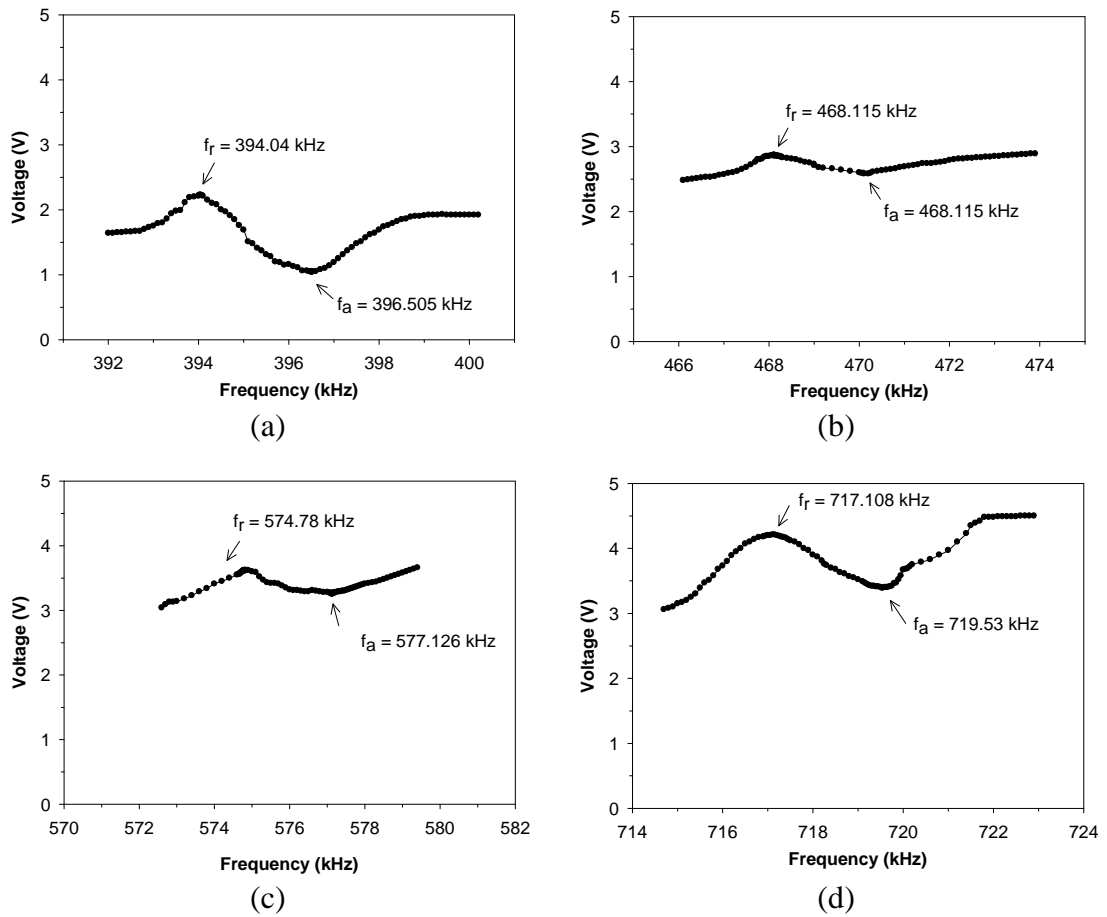


Figure 4.3 Variations of the resonance and antiresonance of the composites with PVDF poled for a stack with (a) 1, (b) 2, (c) 3, and (d) 4 layers.

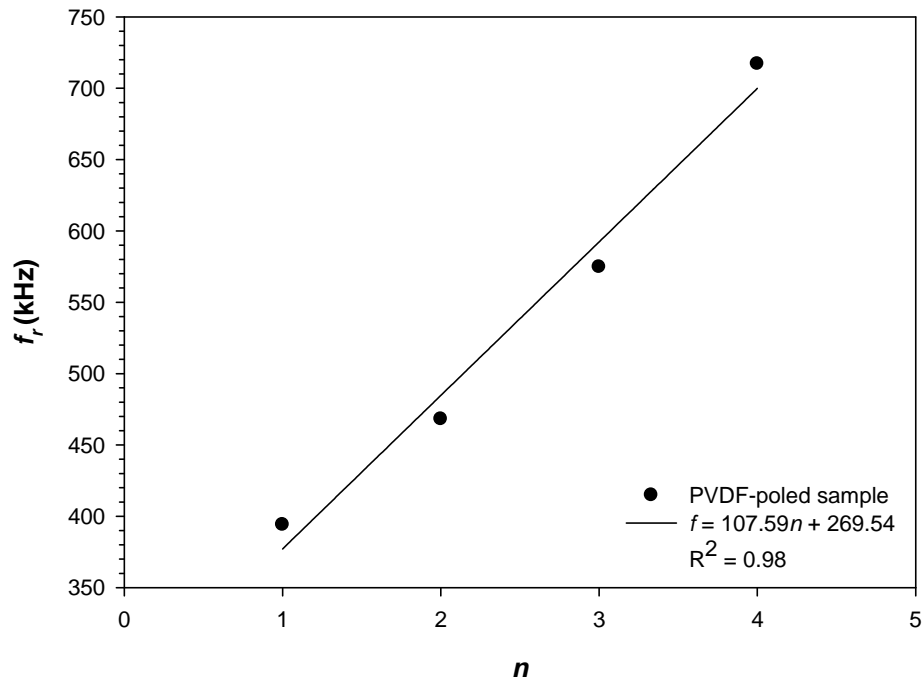


Figure 4.4 Changes in a resonant frequency as a function of the number of layers.

Table 4.1 Percentages of the difference (%diff) between experimental data (EXP) and FEA data for the stack of the BT-PVDF composites with PVDF poled.

n	f_r			f_a		
	EXP	FEA	%diff	EXP	FEA	%diff
1	394,040	395,050	0.26	396,505	395,975	0.13
2	468,115	469,050	0.20	470,107	469,975	0.03
3	574,780	575,424	0.11	577,126	576,350	0.13
4	717,108	717,875	0.11	719,530	718,800	0.10

From Table 4.1, the %diff of f_r and f_a are less than 0.3%. This confirmed the validity of the model used in the FEA. Figure 4.5 summarized all of the k values for the stack corresponded to those in Figures 4.3-4.4 and Table 4.1.

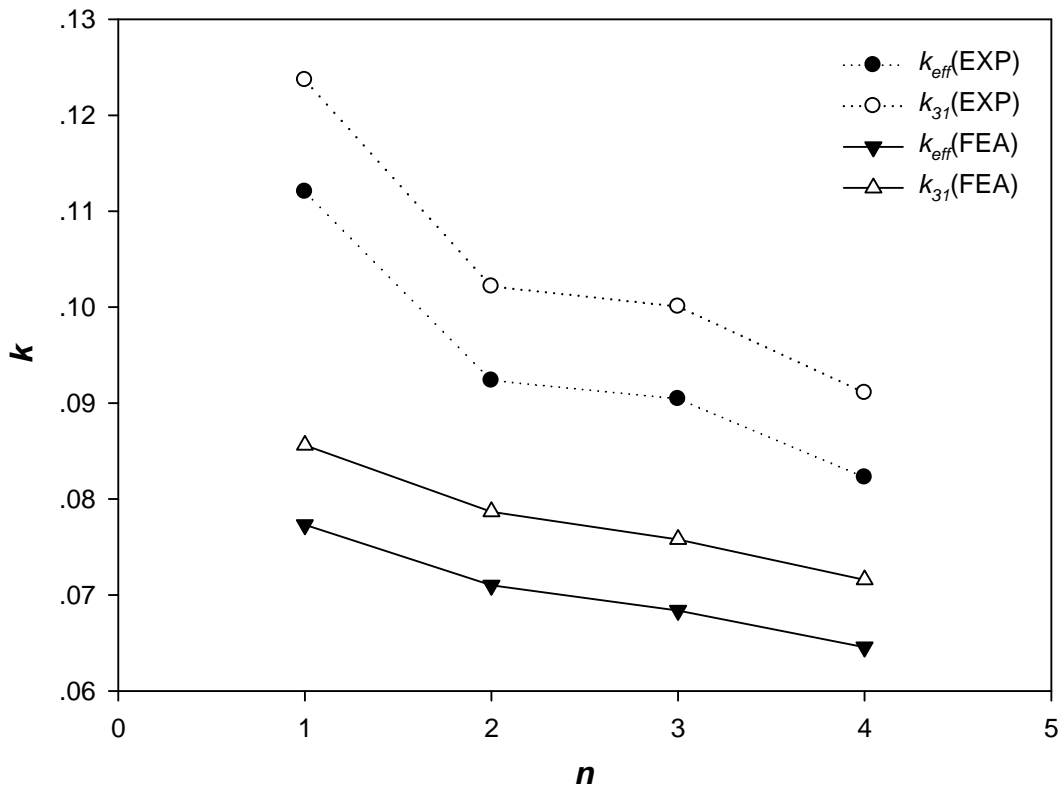


Figure 4.5 Variations of the electromechanical coupling coefficient as a function of the number of the layers in the stack made from the samples with PVDF phased active.

The k_{31} value based on the experimental data is higher than that analyzed by the FEA. This is because the FEA was not taken into account the heterogeneous nature of the diphasic composites. It can be noticed that when n is increased, the k_{31} value is decreased. This stack consisted of the composite with only PVDF active. The polymer normally has a large difference between f_r and f_a (Kwok, 1997). Although n is increased, the k_{31} value of natural (PVDF active) did not increased.

From Figure 4.6, similarly, the experimental k_{31} value was higher than the FEA results. In this case, the value is increased with n . This is because the composite layers were poled in opposite direction. Thus the direction of the dipole moment of each phase was the same and this enhanced the overall piezoelectric

response of the composites. Furthermore, if the directions of the dipole moment in the adjacent layers in the stack were antiparallel, then the impedance of the stack is less than that of the single-layer stack (Wang *et al.*, 2002).

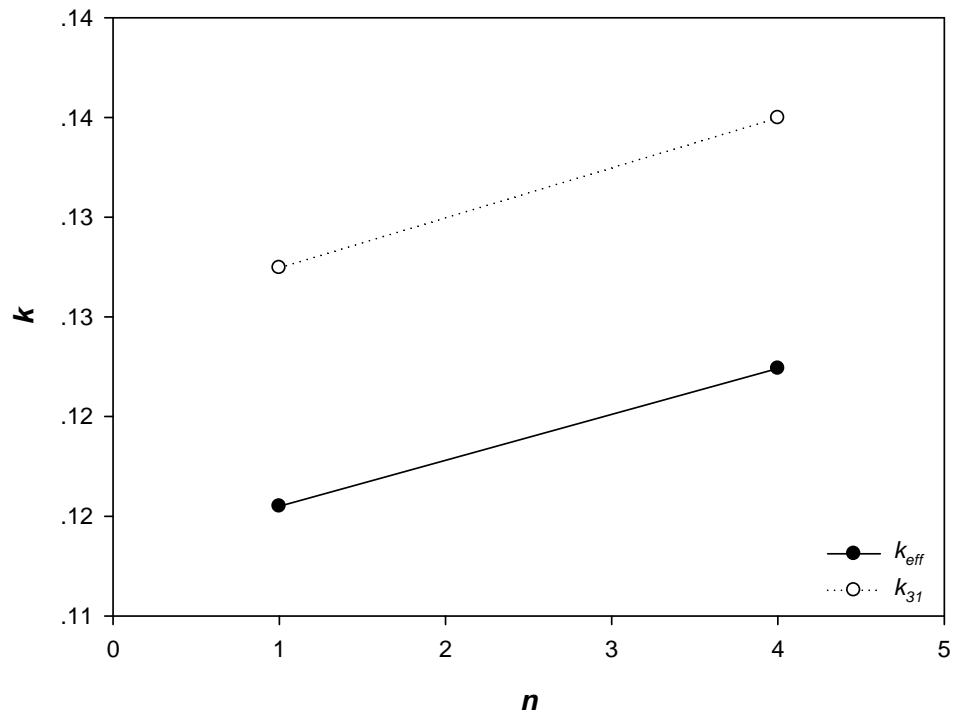


Figure 4.6 Variations of the electromechanical coupling coefficient as a function of the number of layers in the stack made from the samples with both phases active.

This work is interested in the k_{31} coefficient instead of the k_{33} . This is related to the rectangular shape of the sample (Table 2.3). In addition, the elastic compliance of the polymer is relatively high when compared with the ceramic (Chan *et al.*, 2001) therefore the dominant vibration mode for the composite is not longitudinal but lateral deformation (transverse mode). However, if two phases are active, the k_{31} can be increased with increasing layers. For the k_{eff} coefficient, it is always lower than the k_{31} value no matter determined by experiment or FEA. Because it is independent of a shape of piezoelectric materials in the calculation of the k_{eff} coefficient while it is of importance for the k_{31} . It is expected that the piezoelectric stack with both phases active is useful for transducer applications owing to the low

capacitance, low power consumption and stacking-layer dependence of the electromechanical coupling.

Table 4.2 lists the properties of all materials involved in this work. It can be seen that in the material preparation procedure the poling process is an important factor that can affect the overall properties of the 0.15BT-0.85PVDF composites. In turn, the overall properties of the 0.15BT-0.85PVDF composite was dominant by the PVDF matrix.

Table 4.2 A summary of the properties of BaTiO₃, BT-PVDF, and PVDF materials.

Materials	Properties			Reference
	Density (kg/m ³)	Dielectric constant at 1 kHz	Dielectric loss at 1 kHz	
BaTiO ₃	5,800	4,100	0.0035	Sakakibara <i>et al.</i> , 1994 Li <i>et al.</i> , 1995 George <i>et al.</i> , 2008
BT-PVDF	2,425	8.6225	0.0207	This work
PVDF	1,780	8.05	0.0362	Sakakibara <i>et al.</i> , 1994 Varadan <i>et al.</i> , 1989

CHAPTER 5

CONCLUSIONS

5.1 Main Conclusions

In this work, the BT-PVDF composite material of low volume fraction of the ceramic phase dispersed in the host polymer has been prepared. The tape-casted composites with different poling conditions possessed different characteristics. The porous and elastic nature of the polymer dominated the properties of the composites as summarized in Table 5.1.

Table 5.1 Physical and electromechanical properties of the BT-PVDF composites.

Materials	Properties				Reference
	Thickness (mm)	Density (kg/m ³)	Dielectric Constant at 1 kHz	Dielectric Loss at 1 kHz	
BaTiO ₃	-	5,800	4,100	0.0035	[1]-[3]
Composite	0.1	2,425	8.6225*	0.0207*	This work
			8.7530**	0.0138**	
PVDF	-	1,780	8.05	0.0362	[1], [4]

[1] Sakakibara *et al.*, 1994

* PVDF poled

[2] Li *et al.*, 1995

** Both phases poled oppositely

[3] George *et al.*, 2008

[4] Varadan *et al.*, 1989

After poling, the dielectric constant of the composite was increased while the dielectric loss decreased. For the stack with only the PVDF poled active, the resonant (and antiresonant) frequencies, f of a stacking sample were linearly increased with the number of the layers, n as given by:

$$f = 107.59n + 269.54$$

The FEA results of this type of the stack agreed with experimental data from the resonance measurement within an accuracy of about 0.3 %.

This work is interested in the k_{31} coefficient owing to a rectangular shape of a sample and a lateral deformation of the material with increasing number of the layers, the k_{31} coefficient of a stack with PVDF poled was decreased while it was slightly increased in the stack with both phases poled oppositely. A summary was listed in Table 5.2.

Table 5.2 The electromechanical coupling coefficient for all piezoelectric stacks.

Number of layers	k_{31}	
	Poled PVDF	Poled PVDF and BT
1	0.12	0.13
2	0.10	-
3	0.10	-
4	0.09	0.14

5.2 Suggestions and Further Investigations

In the sample preparation, problems arise such as the instability of the rotating rate of a magnetic stirrer and the contamination of dust in preparing procedure. Therefore, tools and equipments must be cleaned and checked before the experiment.

To further reduce errors in the determination of the electromechanical coupling of the composite stack, the number of the layers should be further increased.

Studying the stacked piezoelectric composite transducers by using the 3-D finite element model is of interest for future work.

BIBLIOGRAPHY

- Agilent Solutions for Measuring Permittivity and Permeability with LCR Meters and Impedance Analyzers: Application Note 1369-1. 2006. Agilent Technologies Inc.: USA.
- Ballato, A. 1996. Piezoelectricity: history and new thrusts. Proceeding of the IEEE Ultrasonics Symposium, 1996. San Antonio, TX, November 3-6, 1996. pp. 575-583.
- Burianova, L., Sulc, M. and Prokopova, M. 2001. Determination of the piezoelectric coefficients d_{ij} of PZT ceramics and composites by laser interferometry. Journal of the European Ceramic Society. 21(10-11): 1387-1390.
- Cady, W.G. 1964. Piezoelectricity. Dover Book Publishers: New York.
- Chan, H. L. W., Ng, P. K. L. and Choy, C. L. 1999. Effect of poling procedure on the properties of lead zirconate titanate/vinylidene. Applied Physics Letters. 74(20): 3029-3031.
- Choi, J.-J., Lee, J.-H., Hahn, B.-D., Yoon, W.-H. and Park, D.-S. 2008. Co-firing of PZN-PZT/Ag multilayer actuator prepared by tape-casting method. Materials Research Bulletin. 43(2): 483-490.
- Dasaesamoh, A. 2008. Dielectric Transducer Fabricated from Polymer–Matrix Composite. M. Sc. Thesis. Faculty of Science. Prince of Songkla University, Thailand.
- Dias, C. J. and Das-Gupta, D. K. 1994. Piezo-and pyroelectricity in ferroelectric ceramic-polymer composites. Key Engineering Materials. 92-93: 217-248.

- Dias, C. J. and Das-Gupta, D. K. 1996. Inorganic ceramic/polymer ferroelectric composite electrets. *IEEE Transactions on Dielectrics and Electrical Insulation*. 3(5): 706-734.
- Dos Santos e Lucato, S. L., Lupascu, D. C., Kamlah, M., Rodel, J. and Lynch, C. S. 2001. Constraint-induced crack initiation at electrode edges in piezoelectric ceramics. *Acta Materialia*. 49(14): 2751-2759.
- Ferroperm Piezoceramics. 2003. Ferroperm Piezoceramics A/S: Denmark.
- George, C. N., Thomas, J. K., Kumar, H. P., Suresh, M. K., Kumar, V. R., Wariar, P. R. S., Jose, R. and Koshy, J. 2008. Characterization, sintering and dielectric properties of nanocrystalline barium titanate synthesized through a modified combustion process. *Materials Characterization*. In Press, Corrected Proof.
- Ghouthi, N. E. 2000. Hybrid Modeling of a Traveling Wave Piezoelectric Motor. Ph.D. Thesis, Department of Control Engineering, Aalborg University, Denmark.
- Hajeesaeh, S. and Muensit S. 2006. Theory and measurements for 0-3 BaTiO₃/PVDF composites. *Songklanakarin Journal of Science and Technology*. 2: 413-418.
- Harris, N. R., Hill, M., Torah, R., Townsend, R., Beeby, S., White, N. M. and Ding, J. 2006. A multilayer thick-film PZT actuator for MEMs applications. *Sensors and Actuators A: Physical*. 132(1): 311-316.
- Harrison, J. S. and Ounaies, Z. 2001. Piezoelectric polymers. ICASE Report No. 2001-43. Universities Space Research Association, December, 2001.
- Hirayama, C., Konno, K., Shinbo, H., Li, Z., Grimsditch, M., Foster, C. M., and Chan S.-K. 1996. Dielectric and elastic properties of ferroelectric materials at elevated temperature. *Journal of Physics and Chemistry of Solids*. 57(10): 1433-1438.

- Ikeda T. 1990. *Fundamentals of Piezoelectricity*. Oxford University Press: New York.
- Im, I.-H., Chung, H.-S., Paik, D.-S., Park, C.-Y., Park, J.-J. and Bae, S.-G. 2000. Multilayer piezoelectric actuator with AgPd internal electrode. *Journal of the European Ceramic Society*. 20(7): 1011-1015.
- Jeong, S.-J., Ha, M.-S. and Song, J.-S. 2004. Effect of geometry on properties of multilayer structure actuator. *Sensors and Actuators A: Physical*. 116(3): 509-518.
- Jordan, T. L. and Ounaies, Z. 2001. *Piezoelectric Ceramics Characterization*. ICASE Report No. 2001-28. Universities Space Research Association, September, 2001.
- Kawai, H. 1969. The Piezoelectricity of Poly (vinylidene Fluoride). *Japanese Journal of Applied Physics*. 8: 975-976.
- Kay, H.F. and Vousdan, P. 1949. Symmetry changes in barium titanate at low temperature and their relation to its ferroelectric properties. *Philosophical Magazine*. 7: 1019-1040.
- Koh, J.-H., Jeong, S.-J., Ha, M.-S. and Song, J.-S. 2004. Degradation and cracking behavior of $0.2(\text{PbMg}_{1/3}\text{Nb}_{2/3}\text{O}_3)-0.8(\text{PbZr}_{0.475}\text{Ti}_{0.525}\text{O}_3)$ multilayer ceramic actuators. *Sensors and Actuators A: Physical*. 112(2-3): 232-236.
- Kondo, M., Hida, M., Omote, K., Taniguchi, O., Mita, T., Umemiya, S. and Kurihara, K. 2003. Preparation of $\text{PbNi}_{1/3}\text{Nb}_{2/3}\text{O}_3\text{-PbTiO}_3\text{-PbZrO}_3$ ceramic multilayer actuator with silver internal electrodes. *Sensors and Actuators A: Physical*. 109(1-2): 143-148.

- Kwok, K. W., Chan, H. L. W. and Choy, C. L. 1997. Evaluation of the material parameters of piezoelectric materials by various methods. *IEEE Transactions on Ultrasonics, Ferroelectrics and Frequency Control*. 44(4): 733-742.
- Kwok, K. W., Chan, K. L. W. and Choy, C. L. 1994. Piezoelectric properties of 1-3 composites of PZT in P(VDF-TrFE) copolymer. *Proceedings of the 9th IEEE International Symposium on Applications of Ferroelectrics*. University Park, PA, USA, August 7-10, 1994. pp.194-197.
- Langevin, P. 1950. *Euvres scientifiques de Paul Langevin*, Centre National de la recherche scientifique.
- Lang, S. B. and Das-Gupta, D. K. 2000. Pyroelectricity: Fundamentals and Application. *Ferroelectrics Review*. 2: 217-354.
- Lang, S. B., Das-Gupta, D. K., Hari, S. N. 2001. Pyroelectricity: Fundamentals and applications. *Handbook of Advanced Electronic and Photonic Materials and Devices*. Academic Press: Burlington.
- Lau, S. T., Zhou, Q. F., Kwok, K. W., Chan, H. L. W. and Choy, C. L. 1999. PZT/P(VDF-TrFE) nanocomposites for ultrasonic hydrophone application. *Proceedings of the 10th International Symposium on Electrets*. Athens, September 22-24, 1999. pp. 755-758.
- Li, X.-F. and Guo, S.-H. 2007. Strain incompatibility between dissimilar piezoceramics with a penny-shaped interfacial electrode. *Mechanics of Materials*. 39(11): 977-986.
- Limbong, A. and Guy, I. L. 1998. Pyroelectric hysteresis in PVDF homo-, 65/35 and 75/25 -P(VDF/TrFE) co-polymers, *Thin Solid Films*, 325: 187-191.
- Lovinger, J. A. 1983. *Ferroelectric Polymers*. *Science*. 220: 1115-1121.

- Mason, W. P. and Jafee, H. 1954. Methods for Measuring Piezoelectric, Elastic, and Dielectric Constants of Crystals and Ceramics. *Proceedings of the IRE*. 42(6): pp. 921-930.
- Mistler, R. E., Shanefield, D. J. and Runk, R. B. 1978. Tape Casting of Ceramics. *Ferroelectrics*. 1: 411-448.
- Moulson, A. J. and Herbert, J. M. 1990. *Electroceramics*. Chapman and Hall: New York.
- Newnham, R. E. and Ruschau, G. R. 1991. Smart Electroceramics. *Journal of the American Ceramic Society*. 74(3): 463-480.
- Newnham, R. E., Skinner, D. P. and Cross, L. E. 1978. Connectivity and piezoelectric-pyroelectric composites. *Materials Research Bulletin*. 13(5): 525-536.
- Ng, W. Y., Ploss, B., Chan, H. L. W., Shin, F. G. and Choy, C. L. 2000. Pyroelectric properties of PZT/P(VDF-TrFE) 0-3 composites. *Proceedings of the 2000 12th IEEE International Symposium on Applications of Ferroelectrics*. Honolulu, HI, July 21- Aug 2, 2000. pp.767-770.
- Patil, R., Ashwin, A. and Radhakrishnan, S. 2007. Novel polyaniline/PVDF/BaTiO₃ hybrid composites with high piezo-sensitivity. *Sensors and Actuators A: Physical*. 138(2): 361-365.
- Piezoelectric Ceramics (PIEZOTITE[®]) Sensors. Cat.No.P19E-9, 2008. Murata Manufacturing Co., Ltd.
- Ploss, B., Ng, W.-Y., Chan, H. L.-W., Ploss, B. and Choy, C.-L. 2001. Poling study of PZT/P(VDF-TrFE) composites. *Composites Science and Technology*. 61(7): 957-962.

- Sadiku, M. N. O. 1995. Elements of Electromagnetics. Oxford University Press Inc: Oxford.
- Sakakibara, T., Izu, H., Kura, T., Shinohara, W., Iwata, H. and Kiyama, S. 1994. Development of high-voltage photovoltaic micro-devices for an energy supply to micromachines. Proceedings of the 5th International Symposium on Micro Machine and Human Science. Nagoya, Japan, October 2-4, 1994. pp.71.
- Sherrit, S., Wiederick, H. D. and Mukherjee, B. K. 1992. Non-iterative evaluation of the real and imaginary material constants of piezoelectric resonators. Ferroelectrics. 134: 111-119.
- Smith, W. A. 1989. The role of piezocomposites in ultrasonic transducers. Proceeding of the IEEE Ultrasonics Symposium, 1989. Montreal, Que., Canada, October 3-6, 1989. pp.755-766.
- Smith, W. A. 1993. Modeling 1-3 composite piezoelectrics: hydrostatic response. IEEE Transactions on Ultrasonics, Ferroelectrics and Frequency Control. 40(1): 41-49.
- SPI supplies[®]. 2008. Properties of Cured Silver Films. SPI Supplies and Structure Probe, Inc.
- Transducer Elements: Introduction to Piezo Transducers. Catalog #7b, 2007. Piezo Systems Inc: Cambridge.
- Uchino, K. 1997. Piezoelectric Actuators and Ultrasonic Motors. 2nd ed. Kluwer Academic Publishers: Boston.

- Varadan, V.V., Roh, Y. R., Varadan, V. K. and Trancrell, R. H. 1989. Measurement of all the elastic and dielectric constants of poled PVDF films. Proceedings of the IEEE Ultrasonics Symposium. Montreal, Que., Canada. October 3-6, 1989. pp.727-730.
- Wang, Z. G., Abel, E. W., Mills, R. P. and Liu, Y. 2002. Assessment of multi-layer piezoelectric actuator technology for middle-ear implants. *Mechatronics*. 12(1): 3-17.
- William, D. and Callister, Jr. 2005. *Fundamentals of Materials Science and Engineering: An Integrated Approach*. 2nd ed. John Wiley & Sons Inc: United States of America.
- Zhu, G.-D., Zeng, Z.-G., Zhang, L. and Yan, X.J. 2008. Piezoelectricity in β -phase PVDF crystals: A molecular simulation study. *Computational Materials Science*. In Press, Corrected Proof.

VITAE

Name Mr. Pisan Sukwisut

Student ID 5010220088

Educational Attainment

Degree	Name of Institution	Year of Graduation
B.Sc. (Physics) (Second Class Honors)	Prince of Songkla University	2007

Scholarship Awards during Enrolment

Research Assistant from Faculty of Science, Prince of Songkla University, 2007-2008

List of Publication and Proceedings

Sukwisut, P., Sumethagulwat, W., Pongdara, B. and Muensit, S. 2008. Evaluations of the electromechanical coupling factor for bulk and composite material using a resonance method. The Sixth PSU Engineering Conference. Prince of Songkla University, May 8-9, 2008. pp. 532-536.

Muensit, S., Sukwisut, P., Khaenamkeaw, P. and Lang, S.B. 2008. Piezoelectric coefficients of multilayer $\text{Pb}(\text{Zr}, \text{Ti})\text{O}_3$ thin films. Applied Physics A: Materials Science & Processing. 92(3): 659-663.